CHALMERS

Internal Report 00/4

On the Wall Boundary Condition for Turbulence Models

JONAS BREDBERG

Department of Thermo and Fluid Dynamics
CHALMERS UNIVERSITY OF TECHNOLOGY
Göteborg, Sweden, 2000

On the Wall Boundary Condition for Turbulence Models

JONAS BREDBERG
Department of Thermo and Fluid Dynamics
Chalmers University of Technology

ABSTRACT

This report explains and discuss two main boundary conditions for turbulence models: the integrating and the wall function approach. The report thoroughly derives the law-of-the-wall for both momentum and thermal field. The deviation of these laws from DNS-data is discussed. The Wilcox $k-\omega$ turbulence model constants are derived on the basis of the law-of-the-wall and experiments. Using a simplistic treatment, the low-Reynolds number modifications (damping functions) to the $k-\omega$ model are explained.
Included in the report is also a guideline on the implementation of wall functions, both the standard and the Chieng-Launder two-layer variant.
A new boundary condition for turbulence models combining wall function and integration approach is presented.

Keywords: boundary condition, wall function, turbulence model

Contents

Nomenclature

Latin Symbols

B	Turbulence model constant	$[-]$
C_p	Specific heat	$[J/kgK]$
C	Various constants	$[-]$
C_l	Length-scale constant	$[-]$
C_μ	Turbulence model coefficient	$[-]$
C_f	Skin friction coefficient, $2\tau_w/\rho U_b^2$	$[-]$
D	Hydrualic diameter	$[m]$
e	Rib-size	$[m]$
E	Turbulence model constant	$[-]$
f	Damping function	$[-]$
f, g, F, G	Functions	$[-]$
h	Channel half-height	$[m]$
h	Heat transfer coefficient	$[W/m^2K]$
H	Channel height	$[m]$
i, j	Tensor indices, streamwise: 1 (U) wall normal: 2 (V) spanwise: 3 (W)	$[-]$
k	Turbulent kinetic energy	$[m^2/s^2]$
l	Length scale	$[m]$
Nu	Nusselt number	$[-]$
P	Static pressure	$[N/m^2]$
P	Rib-pitch	$[m]$
P_k	Turbulent production, $\overline{u_i' u_j'}\partial U_i/\partial x_j$	$[m^2/s^3]$
Pr	Prandtl number	$[-]$
Pr_f	Functional Prandtl number	$[-]$
q_i	Heat flux	$[W/m^2]$
R_β, R_k, R_ω	Turbulence model constants	$[-]$
Re	Reynolds number, UH/ν	$[-]$
Re_t	Turbulent Reynolds number, ν_t/ν, $k/(\omega\nu)$, $k^2/(\varepsilon\nu)$	$[-]$
Re_v	Viscous sub-layer Reynolds number, $y_v\sqrt{k_v}/\nu$	$[-]$
Re_τ	u_τ based Reynolds number, $yu_\tau\nu$	$[-]$
S_{ij}	Strain-rate tensor, $1/2(\partial U_i/\partial x_j + \partial U_j/\partial x_i)$	$[s^{-1}]$
T	Temperature	$[K]$
t'	Fluctuating temperature	$[K]$
T_τ	Friction temperature, $(T_w - T)\rho c u_\tau/q_w$	$[K]$
U_i	Velocity	$[m/s]$
u_i'	Fluctuating velocity	$[m/s]$
$\overline{u_i' u_j'}$	Reynolds stresses	$[m^2/s^2]$
u_τ	Friction velocity, $\sqrt{\tau_w/\rho}$	$[m/s]$
u_τ^*	Normalized value: $1000 \times u_\tau/U_b$	$[-]$
x	Streamwise coordinate	$[m]$
y	Wall normal coordinate	$[m]$

Greek Symbols

α	Thermal diffusivity	$[W/m^2K]$
α, α^*	Turbulence model coefficients	$[-]$
β, β^*	Turbulence model coefficients	$[-]$
γ	Turbulence model coefficient	$[-]$
δ	Characteristic length scale	$[m]$
Δ	Cell size	$[m]$
ε	Dissipation rate	$[m^2/s^3]$
η	Normalized wall distance	$[-]$
κ	Van Karman constant	$[-]$
λ	Thermal conductivity, $C_p\mu/Pr$	$[W/mK]$
ν	Kinematic viscosity	$[m^2/s]$
μ	Dynamic viscosity	$[Ns/m^2]$
ρ	Density	$[kg/m^3]$
ω	Specific dissipation rate	$[s^{-1}]$
σ, σ^*	Turbulence model coefficients	$[-]$
τ	Time	$[s]$
τ	Shear stress	$[N/m^2]$
τ_w	Wall shear, ρu_τ^2	$[N/m^2]$

Superscripts

e	Effective value
ϕ^+	Normalized value using u_τ:
T^+	$= T/T_\tau$
U^+	$= U/u_\tau$
y^+	$= yu_\tau/\nu$
k^+	$= k/u_\tau^2$
ε^+	$= \varepsilon\nu/u_\tau^4$
ω^+	$= \omega\nu/u_\tau^2$
τ^+	$= \tau/u_\tau^2$
uv^+	$= \overline{u'v'}/u_\tau^2$
ϕ^*	Normalized value using $\sqrt{k}$:
y^*	$= yC_\mu^{1/4}\sqrt{k}/\nu$ $(k-\varepsilon)$
y^*	$= y\beta^{*1/4}\sqrt{k}/\nu$ $(k-\omega)$

Subscripts

0	Non-modified value
1	First interior node
b	Bulk value
CL	Centerline value
HRN	HRN (logarithmic) part
l	Laminar quantity
LRN	LRN (viscous) part
n	North face value
p	Node value
t	Turbulent quantity
T	Thermal quantity
v	Viscous sub-layer value
w	Wall value
τ	Quantity based on the friction velocity

1 Introduction

One of the most common engineering problems is computing turbulent flows that are influenced by an adjacent wall. Examples of this are flows in turbomachinery, around vehicles, and in pipes. The main two effects of a wall are:

- Damping the wall normal components, making the turbulent flow anisotropic.
- Increasing the production of turbulence through the shearing mechanism in the flow.

The wall gives rise to a boundary layer, where the velocity changes from the no-slip condition at the wall to its free stream value. The variation is usually largest in the near-wall region, and hence the strongest gradients are found here. Similarly, for heat transfer applications, there exists a thermal boundary layer with equally large gradients. Because both heat transfer and friction are computed using gradients of the dependent variable, it is very important to accurately capture this near-wall variation.

The standard method is to apply a very fine mesh close to the wall, to resolve the flow. This method is called the integration method, which necessitates an LRN (low-Reynolds-number) type of turbulence model. At higher Reynolds numbers, the region under the wall influence diminishes. However, because it is equally important to accurately capture the near-wall gradients, a large number of nodes are then necessary. From an engineering point of view, this becomes inconceivable and a function that bridge the near-wall region is instead introduced, thereby significantly reducing the computational requirements. The anticipation is that this can be done with only a small deterioration in the results. This latter approach is denoted the wall function method, which uses an HRN (high-Reynolds-number) type of turbulence model.

2 Near-wall Physics

The near-wall region may be sub-divided into three different areas, Tennekes and Lumley [31]:

- viscous sub-layer $0 < y^+ < 5$
- buffer layer $5 < y^+ < 30$
- inertial sub-layer $30 < y^+ < 200$

The turbulence is negligible in the viscous sub-layer, while the viscous effects are small in the inertial sub-layer. In the buffer layer, however, both turbulent and viscous effects are of importance, see Sahay and Sreenivasan [29] and Fig. 1.

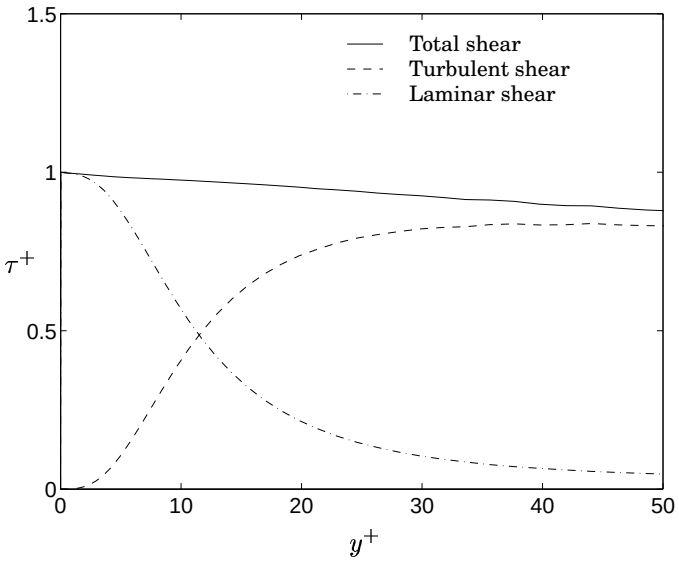

Figure 1: Laminar and turbulent shear in the near wall region. Channel flow, DNS-data, $Re_\tau = 395$ [25].

2.1 Buffer Layer

The maximum turbulent production occurs in the buffer layer at roughly $y^+ = 12$, slightly dependent on the Reynolds number. Due to large variations in the different turbulence source terms, see Figs. 2 and 3, the modelling becomes very difficult. Today there exists no general method for applying a turbulence model, with the first computational interior node located in the buffer layer. Instead of trying to model the behaviour in the buffer layer, the common practise is to place the first near-wall node in either the viscous sub-layer (LRN-models), or in the inertial sub-layer (HRN-models). A viscous approach is valid in the former case, while a turbulent approach is more correct in the latter, for the first interior computational cell.

2.2 Viscous sub-layer

In the viscous sub-layer the following asymptotic relation for the velocity, temperature, turbulence kinetic

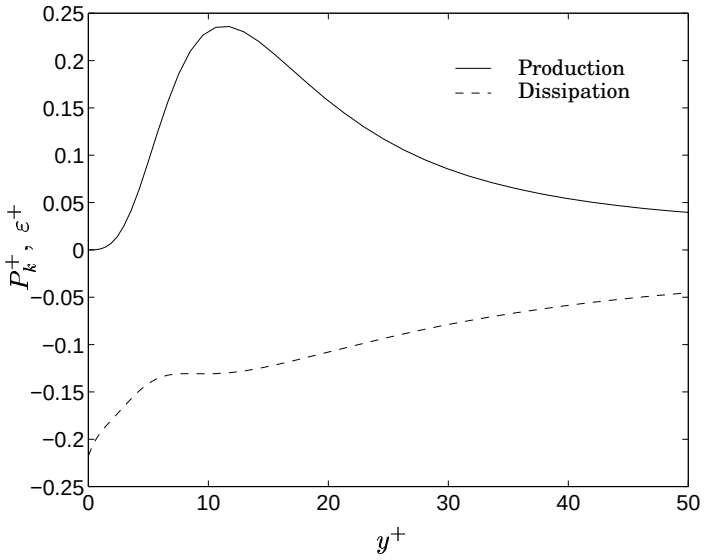

Figure 2: Production and dissipation in the k-equation. Channel flow, DNS-data, $Re_\tau = 395$ [25].

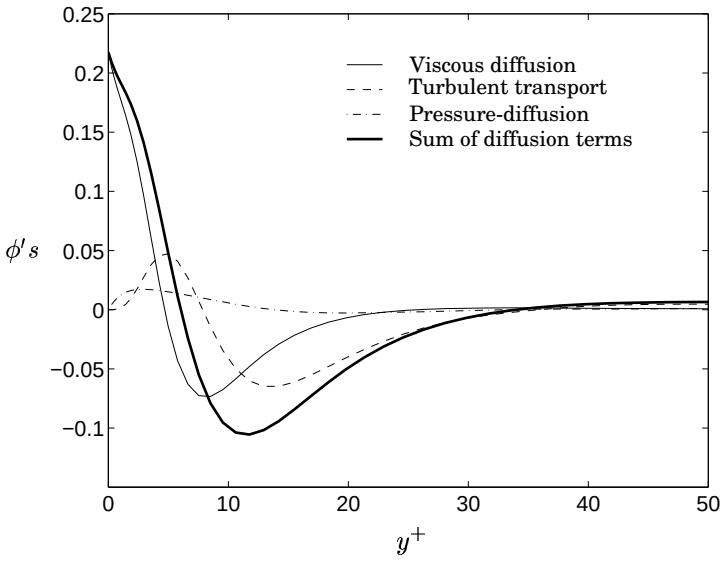

Figure 3: Viscous diffusion, turbulent transport and pressure diffusion terms in the k-equation. Channel flow, DNS-data, $Re_\tau = 395$ [25].

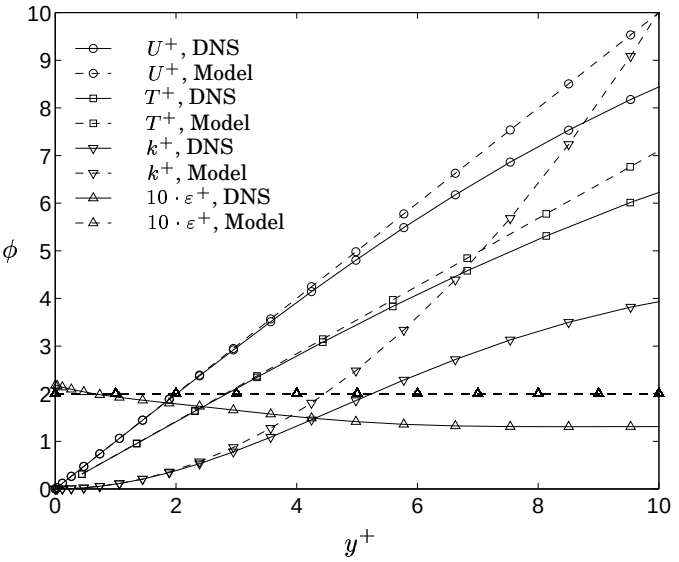

Figure 4: Near-wall variation in U, T, k, ε. Channel flow, DNS-data, $Re_\tau = 395$ [25].

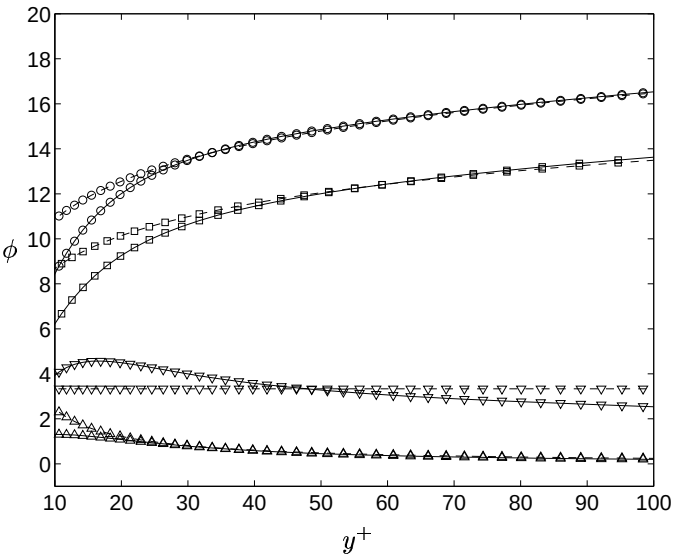

Figure 5: Variation in U, T, k, ε in the inertial sub-layer. Channel flow, DNS-data, $Re_\tau = 395$ [25]. Labels as in Fig. 4

energy and dissipation rate is valid:

$$U^+ = y^+ \quad (1)$$
$$T^+ = Pry^+ \quad (2)$$
$$k^+ = C_1 y^{+2} \quad (3)$$
$$\varepsilon^+ = C_2 \quad (4)$$

where the variables are normalised $()^+$ according to the nomenclature.

The constants used in the relation for the turbulence quantities in Fig. 4 are $C_1 = 0.1$ and $C_2 = 0.2$, which gives close agreement in the wall vicinity. As can be seen from the figure, the relations for the velocity, temperature and dissipation rate are a fair approximation, even up to $y^+ = 10$, although the model for turbulent kinetic energy yields a strong over-estimation for larger y^+ values. In light of this, a plausible turbulence model would be to assume a variation in both the velocity profile and the dissipation rate, while the turbulent kinetic energy should be solved and not set *a priori*.

2.3 Inertial Sub-layer

The inertial sub-layer is the region observed from around $y^+ = 30$ and outwards, where the assumed variations are, see e.g. Wilcox [36]:

$$U^+ = \frac{1}{\kappa} \ln y^+ + B \quad (5)$$
$$T^+ = \frac{1}{\kappa_T} \ln y^+ + B_T \quad (6)$$
$$k^+ = \frac{1}{\sqrt{C_\mu}} \quad (7)$$
$$\varepsilon^+ = \frac{\nu}{u_\tau \kappa y} \quad (8)$$

where $\kappa = 0.41$, $C_\mu = 0.09$ and $B = 5.25$ are justified by DNS-data. For air, Kays and Crawford [20] give the following values: $\kappa_T = Pr_t/\kappa = 0.48$ and $B_T = 3.9$ in the relation for the temperature. The inertial sub-layer is also denoted the logarithmic (log) region, due to the above characteristic profiles, which feature a logarithmic behaviour.

The models assumed for the inertial sub-layer are compared with DNS-data in Fig. 5. There is excellent agreement for both the velocity and temperature relations beyond $y^+ > 30$. The turbulent quantities are however less accurate, and the assumed constant values for the turbulence kinetic energy are not correct. At $y^+ = 100$ there is a descrepancy of around 25% when using either Eq. 7 or 8 as compared with DNS-data.

3 Law-of-the-Wall

The variation in the different parameters in the logarithmic region, postulated in the previous section, is based on the **law-of-the-wall** and its consequences. Below, the law-of-the-wall for both momentum and temperature are derived. The latter is an extension of the former, based on the modified Reynolds analogy. The assumed variation in the turbulence quantities can only be proven, see section 3.3 and 3.4, in conjunction with a specific turbulence model. In this paper the Wilcox $k-\omega$ turbulence model is used. The constants included are derived in section 3.4.

3.1 Momentum

Assuming that a Couette-like flow prevails, the following simplifications can be made to the momentum equations:

- 1D flow, with variation only in the wall-normal direction: $\phi = f(y)$.
- Fully developed flow with zero gradients in the streamwise direction; $\partial/\partial x = 0$, apart from a pressure gradient: $p(x, y)$.
- Negligible convection.

The streamwise $(x-)$ and the wall-normal $(y-)$ momentum equation then reduces to:

$$0 = -\frac{\partial P}{\partial x} + \frac{d}{dy}\left(\mu\frac{dU}{dy} - \rho\overline{u'v'}\right) \tag{9}$$

$$0 = -\frac{\partial P}{\partial y} + \frac{d}{dy}\left(-\rho\overline{v'v'}\right) \tag{10}$$

Because Eq. 10 is now an ordinate differential, it can easily be integrated to yield:

$$P(x, y) = -\rho\overline{v'v'} + P_w(x) \tag{11}$$

Inserting this into Eq. 9, assuming that $\partial\rho\overline{v'v'}/\partial x = 0$, the integration yields:

$$\begin{aligned} 0 &= -\int \frac{dP_w}{dx}dy + \int \frac{d}{dy}\left(\mu\frac{dU}{dy} - \rho\overline{u'v'}\right)dy \quad \Rightarrow \\ 0 &= -\frac{dP_w}{dx}y + \mu\frac{dU}{dy} - \rho\overline{u'v'} - \tau_w \end{aligned} \tag{12}$$

At the centreline $(y = h)$ – of a channel – the shear stress, $\rho\overline{u'v'}$, and the velocity gradient, $\partial U/\partial$, are zero and the pressure gradient can consequently be established as:

$$\frac{dP_w}{dx} = -\frac{1}{h}\tau_w \tag{13}$$

The shear stress variation can thus be written as:

$$\underbrace{\mu\frac{dU}{dy}}_{\text{laminar}} \underbrace{-\rho\overline{u'v'}}_{\text{turbulent}} = \left(1 - \frac{y}{h}\right)\tau_w \tag{14}$$

Note that $\overline{u'v'}$ is negative and hence the left-handside (LHS) of Eq. 14 – i.e. the total shear stress – linearly decreases from the wall to the centre of the channel. This is of course in excellent agreement with DNS-data for fully developed flow, see Fig. 1.

If Eq. 14 is normalised with the friction velocity, u_τ, and a length-scale based on wall quantities:

$$y^+ \equiv \frac{y u_\tau}{\nu} \tag{15}$$

The relation becomes:

$$\frac{dU^+}{dy^+} - \overline{uv^+} = 1 - \frac{y^+}{Re_\tau} \tag{16}$$

where the turbulent Reynolds number is defined as: $Re_\tau = u_\tau h/\nu$.

For a large ratio of Re_τ/y^+, one can assume that the total shear is constant. Hence the velocity and shear stress can be written as a function of y^+ only:

$$U^+ = f(y^+) \tag{17}$$

$$-\overline{uv^+} = g(y^+) \tag{18}$$

These relations are called the '**law-of-the-wall**' expressed in inner variables, as proposed by Prandtl [27].

If the inertial sub-layer is instead approached from the core of the flow, and the equation is normalised with the mean flow length scale:

$$\eta \equiv \frac{y}{h} \tag{19}$$

and the friction velocity, the following relation is given:

$$\frac{1}{Re_\tau}\frac{dU^+}{d\eta} - \overline{uv^+} = 1 - \eta \tag{20}$$

For large Re_τ the first term on the LHS can be neglected and thus the relation reduces to:

$$-\overline{uv^+} = G(\eta) \tag{21}$$

Note however that this does not give a relation for U itself. On the basis of purely dimensional grounds, it is possible to establish a relation for the velocity profile, similar to Eq. 17, although as a function of the wall distance in outer variables only, van Karman [33]:

$$\frac{U - U_{CL}}{u_\tau} = F(\eta) \tag{22}$$

where U^+_{CL} is the centreline velocity and U^+ is the defect velocity. This relation is called the **'velocity-defect law'**, Tennekes and Lumley [31]

Somewhere in the flow it is plausible to assume that both relations for the U-velocity hold. Differentiating Eqs. 17 and 22 and adding a proportional constant as done by Clauser [9] gives:

$$\eta\frac{dF}{d\eta} = y^+\frac{df}{dy^+} = \frac{1}{\kappa} \tag{23}$$

where κ is the von Karman constant, equal to $0.4 - 0.42$. Integrating the latter relation gives:

$$f = \frac{1}{\kappa}\ln(y^+) + B \tag{24}$$

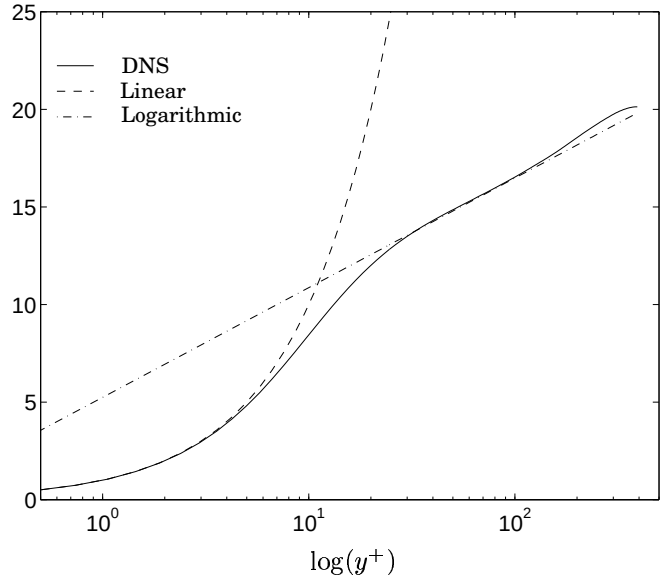

Figure 6: U-velocity profile with linear and log-law approximation. Channel flow, DNS-data, $Re_\tau = 395$ [25].

where B is an integration constant, which is given a value of $5 - 5.5$ based on experimental data. The logarithmic law or log-law for the velocity is thus:

$$U^+ = \frac{1}{0.41}\ln(y^+) + 5.25 \tag{25}$$

The velocity profile using this relation and the linear relation, $U^+ = y^+$, is compared with DNS-data in Fig. 6. The intercept between the two laws is found at $y^+ = 11$, located in the buffer layer, which is, as is obvious from the figure, not accurately modelled by either of the equations.

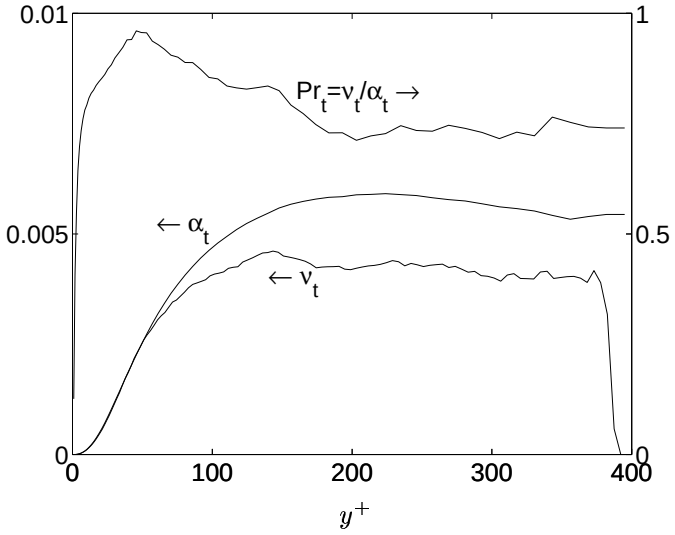

Figure 7: Diffusivities and turbulent Prandtl number for air. Channel flow, DNS-data $Re_\tau = 395$ [25], [18].

3.2 Energy/Temperature

An inspection of the structure of the governing equation for energy and momentum reveals that the near-wall

mechanisms would be similar only if the Prandtl numbers (both the molecular and turbulent) are unity. The definition of the turbulent Prandtl number is:

$$Pr_t \equiv \overline{u'v'}\frac{dT}{dy}/\overline{v't'}\frac{dU}{dy} \tag{26}$$

The turbulent Prandtl number and the turbulent momentum diffusivity, ν_t, and turbulent thermal diffusivity, α_t, are plotted in Fig. 7. The definitions of ν_t and α_t are:

$$\nu_t \equiv \frac{\overline{u'v'}}{dU/dy} \tag{27}$$

$$\alpha_t \equiv \frac{\overline{v't'}}{dT/dy} \tag{28}$$

Reynolds, in an attempt to describe the heat exchange process, proposed a model which is based on similarities between the momentum and energy transfer. Reynolds' analogy presupposes that the two diffusivities, ν_t and α_t, are equal and hence, from Eq. 26, that the turbulent Prandtl number is unity, $Pr_t = 1$. For a fluid with a unit molecular Prandtl number, $Pr = 1$, this would result in identical temperature and velocity profiles. The validity of the Reynolds analogy can be observed in Fig. 7. As noted the assumption of a constant Pr_t can only be acceptable in the inertial sub-layer, and with a value less than unity, $Pr_t \approx 0.8$.

Although the validity of the Reynolds analogy is limited, there still exists a strong similarity between the velocity field and the temperature field, which implies that there could exist a corresponding law-of-the-wall for the thermal field.

With the same assumptions as for the momentum equation, i.e. 1D fully developed flow field and thermal field, the energy (temperature) equation in the wall-normal direction can be simplified to:

$$0 = \frac{1}{C_p}\frac{dq}{dy} = \frac{d}{dy}\left(\alpha\frac{dT}{dy} - \overline{v't'}\right) \tag{29}$$

where C_p is the specific heat of the fluid and α is the (viscous) thermal diffusivity.
Note that the pressure gradient, contrary to the momentum equation, does not appear in this equation. If a non-negligible pressure gradient were present, much of the similarity between the momentum and energy equation would be lost.
Assuming that the turbulent heat flux, $\overline{v't'}$, can be described with the turbulent thermal diffusivity and the turbulent Prandtl number, the relation can be re-written as:

$$0 = \frac{d}{dy}\left[\left(\frac{\mu}{Pr} + \frac{\mu_t}{Pr_t}\right)\frac{dT}{dy}\right] \tag{30}$$

When integrating this equation from the wall to the centre of the channel, the heat flux is found as:

$$C = \left(\frac{\mu}{Pr} + \frac{\mu_t}{Pr_t}\right)\frac{dT}{dy} \tag{31}$$

where the integration constant, C, is a function of the heat flux applied at the wall:

$$C = -\frac{q_w}{C_p} \tag{32}$$

	Pr	y^+_{crit}
Air:	0.7	13.2
Water:	5.9	7.55

Table 1: Critical y^+ values, air and water

Re-arranging and integrating once more gives:

$$\begin{aligned} -\frac{q_w}{C_p} &= \left(\frac{\mu}{Pr} + \frac{\mu_t}{Pr_t}\right)\frac{dT}{dy} \qquad \Rightarrow \\ \int_{T_w}^{T} dT &= -\frac{q_w}{C_p}\int_0^y \frac{dy}{\mu/Pr + \mu_t/Pr_t} \end{aligned} \tag{33}$$

On introducing normalised values:

$$y^+ \equiv \frac{yu_\tau}{\nu} \tag{34}$$

$$T^+ \equiv \frac{(T_w - T)\rho C_p u_\tau}{q_w} \tag{35}$$

and re-arranging, the equation yields:

$$T^+ = \int_0^{y^+} \frac{dy^+}{1/Pr + (\nu_t/\nu)/Pr_t} \tag{36}$$

This gives the variation of T^+ as a function of y^+, although in an integrated form, which is not preferable when making comparisons with the law-of-the-wall for the momentum equation. The formulation could however be simplified if it were possible to divide the near-wall region into a laminar and a turbulent layer. In the case of the momentum equation, the velocity profile follows approximate a linear relation in the viscous sub-layer (laminar) region and a logarithmic relation in the inertial sub-layer (turbulent) region. If the thermal field behaved similarly, the above integral can be divided and integrated successfully. The location of this partition depends on the molecular Prandtl number, which for a value of unity would be identical to that of the momentum equation, i.e. $y^+ = 11$. For a lower value of the Prandtl number, e.g. air ($Pr = 0.71$), this critical value will be higher, with the opposite being true for a high Prandtl number fluid, e.g. water ($Pr = 5.9$). Examples of these cross-over locations, or critical y^+ values, are given in table 1, see also Kays and Crawford [20]. Taking the value for air, the two integrals would be:

$$T^+ = \int_0^{13.2} Pr\,dy^+ + \int_{13.2}^{y^+} \frac{dy^+}{(\nu_t/\nu)/Pr_t} \tag{37}$$

where it was assumed that the turbulent part could be neglected in the first integral and the laminar part in the second integral. The first integral is easily integrated to yield the linear-law for the temperature as:

$$T^+_{0\to 13.2} = Pr\,y^+ \tag{38}$$

However the second part can only be integrated if the variation in ν_t/ν and Pr_t is known. In the inertial sub-layer the turbulent Prandtl number can with acceptable accuracy be assumed constant. The ratio ν_t/ν, or the

turbulent Reynolds number, can be approximated using the mixing-length theory, which gives:

$$\nu_t = u_\tau \kappa y \Rightarrow \qquad \frac{\nu_t}{\nu} = \kappa y^+ \tag{39}$$

Adopting this and evaluating the integral yields:

$$T^+_{13.2 \to y^+} = Pr_t \int_{13.2}^{y^+} \frac{dy^+}{\kappa y^+} = \frac{Pr_t}{\kappa} \ln\left(\frac{y^+}{13.2}\right) \tag{40}$$

Thus the law-of-the-wall for the thermal field, or the temperature log-law, is, adding Eq. 38 and 40

$$T^+ = 13.2Pr + \frac{Pr_t}{\kappa} \ln\left(\frac{y^+}{13.2}\right) = 2.075 \ln(y^+) + 3.9 \tag{41}$$

where the constants are found by using properties for air ($Pr = 0.7$ and $Pr_t = 0.85$) and the van Karman constant, $\kappa = 0.41$.

The two formulations, the linear-law and the log-law, are compared with DNS-data in Fig. 8. Similar to the momentum (velocity) model, the agreement is less accurate in the buffer layer where neither equation gives acceptable performance. For air, the cross-over between the two laws is found at $y^+ = 13.2$, and hence the laminar thermal layer extends further out than the laminar momentum layer.

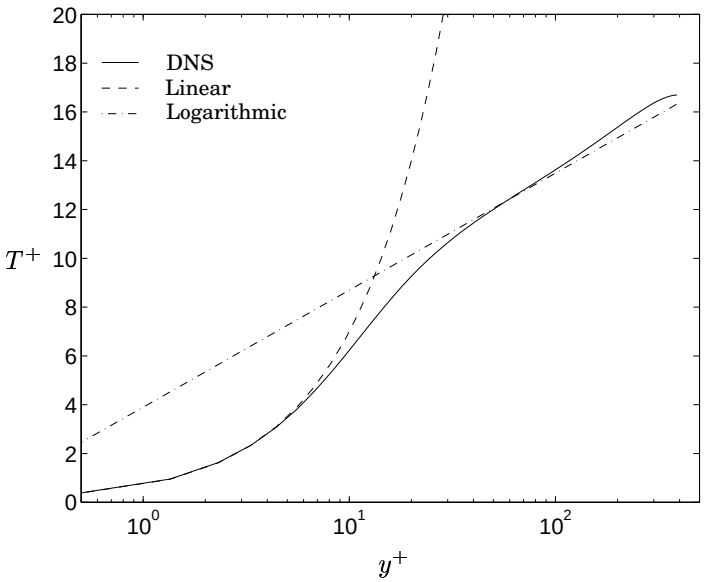

Figure 8: Temperature profile with linear and log-law approximation. Channel flow, DNS-data, $Re_\tau = 395$ [18].

3.3 Turbulence

There is a number of different approaches to the turbulent law-of-the-wall, or log-laws, where the derivations below mirror that of Wilcox [36]. If 1D fully developed flow is assumed, and the pressure influence is neglected (even in the streamwise direction) the Wilcox $k-\omega$[1] HRN model (see section 3.5) reduces in the inertial sub-layer to:

$$0 = \frac{d}{dy}\left(\nu_t \frac{dU}{dy}\right) \tag{42}$$

$$0 = \nu_t \left(\frac{dU}{dy}\right)^2 - \beta^* \omega k + \sigma^* \frac{d}{dy}\left(\nu_t \frac{dk}{dy}\right) \tag{43}$$

$$0 = \gamma \left(\frac{dU}{dy}\right)^2 - \beta \omega^2 + \sigma \frac{d}{dy}\left(\nu_t \frac{d\omega}{dy}\right) \tag{44}$$

$$\nu_t = \frac{k}{\omega} \tag{45}$$

where the laminar viscosity in the diffusion terms is neglected. Note that the neglected pressure gradient in the momentum equation (Eq. 42) is a severe limitation in the following derivation. This makes the wall function approach even more questionable for the turbulent quantities than for the velocity field.

The above equations can be satisfied in the inertial sub-layer with the following set of wall functions, see Wilcox [36]:

$$U = \frac{u_\tau}{\kappa} \ln\left(\frac{y u_\tau}{\nu}\right) + B \tag{46}$$

$$k = \frac{u_\tau^2}{\sqrt{\beta^*}} \tag{47}$$

$$\omega = \frac{u_\tau}{\sqrt{\beta^*}\kappa y} \tag{48}$$

$$\nu_t = u_\tau \kappa y \tag{49}$$

These relations can be proven by re-inserting them into the above transport equations. Using Eqs. 49 and 46 in Eq. 42 yields:

$$\begin{aligned} 0 &= \frac{d}{dy}\left[u_\tau \kappa y \frac{d}{dy}\left(\frac{u_\tau}{\kappa} \ln\left(\frac{y u_\tau}{\nu}\right) + B\right)\right] = \\ &= \frac{d}{dy}\left(u_\tau \kappa y \frac{u_\tau}{\kappa} \frac{1}{y}\right) = \frac{d}{dy}\left(u_\tau^2\right) = 0 \end{aligned} \tag{50}$$

Thus these wall functions satisfy the momentum equation. Eqs. 46, 47, 48 and 49 are substituted into Eq. 43 which gives:

$$\begin{aligned} 0 &= u_\tau \kappa y \left[\frac{d}{dy}\left(\frac{u_\tau}{\kappa} \ln\left(\frac{y u_\tau}{\nu}\right)\right)\right]^2 - \beta^* \frac{u_\tau}{\sqrt{\beta^*}\kappa y} \frac{u_\tau^2}{\sqrt{\beta^*}} + \\ &+ \sigma^* \frac{d}{dy}\left[u_\tau \kappa y \frac{d}{dy}\left(\frac{u_\tau}{\sqrt{\beta^*}}\right)\right] = \\ &= u_\tau \kappa y \left(\frac{u_\tau}{\kappa} \frac{1}{y}\right)^2 - \frac{u_\tau^3}{\kappa y} + 0 = \frac{u_\tau^3}{\kappa y} - \frac{u_\tau^3}{\kappa y} = 0 \end{aligned} \tag{51}$$

The turbulent kinetic energy equation is also fulfilled.

Turning to the dissipation rate equation, Eq. 44, and

[1] Note that the log-law may be derived for any turbulence model. The Wilcox $k-\omega$ is used however, because it will later be used in the description of blending turbulence model.

using the wall functions, Eqs. 46, 47, 48 and 49, gives:

$$\begin{aligned}
0 =& \gamma\left[\frac{d}{dy}\left(\frac{u_\tau}{\kappa}\ln\left(\frac{yu_\tau}{\nu}\right)\right)\right]^2 - \beta\left(\frac{u_\tau}{\sqrt{\beta^*}\kappa y}\right)^2 + \\
&+ \sigma\frac{d}{dy}\left[u_\tau\kappa y\frac{d}{dy}\left(\frac{u_\tau}{\sqrt{\beta^*}\kappa y}\right)\right] = \gamma\left(\frac{u_\tau}{\kappa}\frac{1}{y}\right)^2 - \\
&- \beta\frac{u_\tau^2}{\beta^*\kappa^2 y^2} + \sigma\frac{d}{dy}\left(u_\tau\kappa y\frac{u_\tau}{\sqrt{\beta^*}\kappa}\frac{-1}{y^2}\right) = \\
=& \left(\frac{u_\tau}{\kappa y}\right)^2\left(\gamma - \frac{\beta}{\beta^*}\right) + \sigma\frac{u_\tau^2}{\sqrt{\beta^*}}\frac{1}{y^2} = \\
=& \left(\gamma - \frac{\beta}{\beta^*}\right) + \kappa^2\frac{\sigma}{\sqrt{\beta^*}} = 0 \qquad \Rightarrow \\
\kappa^2 =& \frac{\sqrt{\beta^*}}{\sigma}\left(\frac{\beta}{\beta^*} - \gamma\right)
\end{aligned} \tag{52}$$

To satisfy the last relation, it is necessary to establish an identity between coefficients κ, β, β^*, γ and σ.

3.4 Turbulence Model Constants

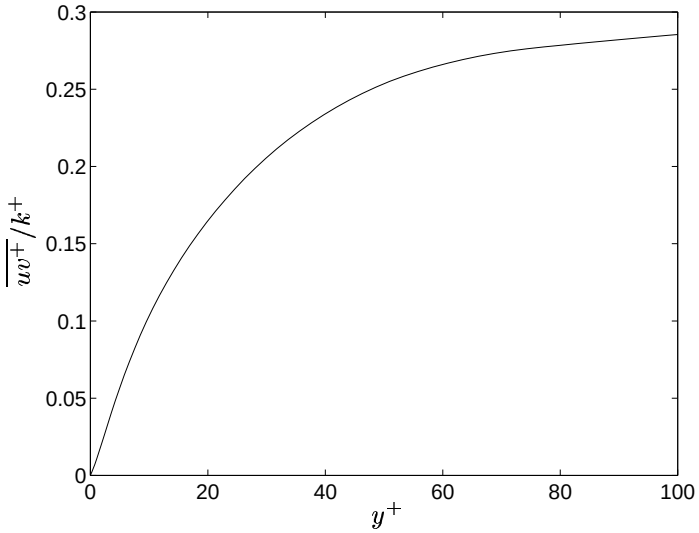

Figure 9: Shear stress to turbulent kinetic energy. Channel flow, DNS-data, $Re_\tau = 395$ [25].

3.4.1 Coefficient, β^*

Experiments have shown that the shear stress and the turbulent kinetic energy is related as

$$\tau_{xy} \approx 0.3\rho k \tag{53}$$

in the logarithmic region. The validity of this approximation is shown in Fig. 9. If the shear stress can be assumed to be constant and the laminar part is neglected, then:

$$\tau_{xy} = \underbrace{\tau_l}_{\sim 0} + \tau_t = \tau_w \equiv \rho u_\tau^2 \tag{54}$$

where the friction velocity is defined as $u_\tau \equiv \sqrt{\tau_w/\rho}$. Now, using the relation for the turbulent kinetic energy from Eq. 47 and the measured relation of above, Eq. 53, we can write the coefficient as:

$$\begin{aligned}
&\rho u_\tau^2 = 0.3\rho k = 0.3\rho\frac{u_\tau^2}{\sqrt{\beta^*}} \qquad \Rightarrow \\
&\beta^* = 0.09
\end{aligned} \tag{55}$$

3.4.2 Coefficient, β

By studying how grid-turbulence dies out, it is possible to determine the coefficient, β. In decaying turbulence, the turbulence equations simplify to:

$$\frac{dk}{d\tau} = -\beta^*\omega k \tag{56}$$

$$\frac{d\omega}{d\tau} = -\beta\omega^2 \tag{57}$$

Solving this equation system gives:

$$k \sim \tau^{-\beta*/\beta} \tag{58}$$

Measurements [32] indicate that the turbulence kinetic energy decays as:

$$k \sim \tau^{-n}, \qquad n = 1.25 \pm 0.06 \tag{59}$$

and hence the ratio $\beta^*/\beta = 1.25 \pm 0.06$. With $\beta^* = 0.09$ from above, the correct value for β would be:

$$\beta = 0.069 - 0.076$$

The $k-\omega$ turbulence model by Wilcox [34] gives this coefficient the value of $\beta = 3/40 = 0.075$.

3.4.3 Coefficients, σ, σ^*

There is no consensus within the turbulence modelling community about the values for these coefficients. Different Schmidt numbers are arrived at depending on the set of experimental data used. In recent years there has also been a greater tendency to introduce modifications for these coefficients, and the values used in turbulence models thus differs. The two Schmidt numbers for the $k-\omega$ model [34] are optimised to:

$$\sigma = \frac{1}{2}$$

$$\sigma^* = \frac{1}{2}$$

3.4.4 Coefficient, γ

The final coefficient, γ, is set using the deduced relation from the specific dissipation rate equation, Eq. 52. With $\kappa = 0.41$ and the above constants, γ is calculated as:

$$\gamma = \frac{\beta}{\beta^*} - \frac{\kappa^2\sigma}{\sqrt{\beta^*}} = \frac{0.075}{0.09} - \frac{0.41^2 0.5}{\sqrt{0.09}} = 0.553 \tag{60}$$

In the Wilcox $k-\omega$ model γ is given the value of $5/9 = 0.555$.

3.5 HRN Turbulence Model

On the basis of the above derived turbulence constants it is possible to write the Wilcox $k-\omega$ model as follows:

$$\nu_t = \frac{k}{\omega} \tag{61}$$

$$\frac{Dk}{D\tau} = P_k - \beta^* k\omega + \frac{\partial}{\partial x_j}\left[(\nu + \sigma^* \nu_t)\frac{\partial k}{\partial x_j}\right] \tag{62}$$

$$\frac{D\omega}{D\tau} = \gamma\frac{\omega}{k}P_k - \beta\omega^2 + \frac{\partial}{\partial x_j}\left[(\nu + \sigma \nu_t)\frac{\partial \omega}{\partial x_j}\right] \tag{63}$$

with the constants as derived earlier:

$$\gamma = 5/9,\ \beta^* = 9/100,\ \beta = 3/40,\ \sigma^* = 1/2,\ \sigma = 1/2$$

4 Modelling Near-wall Turbulence

With respect to wall treatment, there are two different categories of turbulence models. The first are the LRN-models, which use a refined mesh close to wall in order to resolve all the important physics. The second method employs the HRN-models, which bridge the near-wall region using wall functions. The latter approach is of course less demanding of computer resources, but a significant amount of information is lost.

The wall function method is based on the previously mentioned 'law-of-the-wall' and is strictly valid only in the inertial sub-layer (log-layer), 1D fully developed flow, where the pressure gradient can be neglected. The situations in which all these simplifications are fulfilled are relatively few, and the predictions made using wall function or HRN turbulence models are thus generally less accurate than those that apply the integrated method of LRN turbulence models.

The reason why there is still an interest in wall functions is the need to reduce computational requirements, as well as the better numerical stability and convergence speed. If it were possible to improve the predictions using wall functions, more problems of engineering interest could be solved with academic quality, resulting in fewer safety margins and less need of experimental validation when designing new products.

The previous section derived the commonly used wall functions based on the law-of-the-wall, while this section will focus on alternatives to these wall functions.

However, before embarking on strategies in constructing wall functions, it is beneficial to study the near-wall physics from a modelling point of view. Attention is first directed towards the LRN-models and their damping functions.

4.1 LRN-models: Integration Method

It is generally implied that a turbulence model that can integrated toward the wall is denoted a LRN turbulence model. This is usually the same as including damping functions for certain terms in the turbulence equations. The damping functions are introduced to represent the viscous effects near a wall. Successfully devised damping functions should reproduce the correct asymptotic behaviour in the limit of a wall. The exception to the rule that 'damping function $\equiv$ LRN' is the HRN $k-\omega$ turbulence model by Wilcox (1988) [34]. This model can, like the LRN version [35], be integrated to the wall but without the need to employ damping functions. In this paper the identity of damping function and LRN is used for these models as well. This nomenclature thus helps to distinguish them, with the '88 model somewhat erroneously denoted the HRN $k-\omega$ and the '93 model the LRN $k-\omega$ model.

The Wilcox HRN $k-\omega$ model was given in the previous

section and the LRN $k-\omega$ model [35] is:

$$\nu_t = \alpha^* \frac{k}{\omega} \tag{64}$$

$$\alpha^* = \frac{\alpha_0^* + Re_t/R_k}{1 + Re_t/R_k} \tag{65}$$

$$\frac{Dk}{D\tau} = P_k - \beta^* k\omega + \frac{\partial}{\partial x_j}\left[(\nu + \sigma^* \nu_t)\frac{\partial k}{\partial x_j}\right] \tag{66}$$

$$\beta^* = \frac{9}{100}\frac{5/18 + (Re_t/R_\beta)^4}{1 + (Re_t/Re_\beta)^4} \tag{67}$$

$$\frac{D\omega}{D\tau} = \alpha\frac{\omega}{k}P_k - \beta\omega^2 + \frac{\partial}{\partial x_j}\left[(\nu + \sigma\nu_t)\frac{\partial \omega}{\partial x_j}\right] \tag{68}$$

$$\alpha = \frac{1}{\alpha^*}\frac{5}{9}\frac{\alpha_0 + Re_t/R_\omega}{1 + Re_t/R_\omega} \tag{69}$$

where the turbulent Reynolds number is defined as $Re_t = k/(\nu\omega)$ and the turbulent production as $P_k = 2\nu_t S_{ij}\partial U_i/\partial x_j$. The coefficients involved are:

$$\alpha_0 = 1/10,\ \alpha_0^* = \beta/3,\ \beta = 3/40,\ \sigma^* = 1/2,\ \sigma = 1/2$$
$$R_\beta = 8, \qquad R_k = 27/10, \qquad R_\omega = 6$$

This model reduces to the HRN $k-\omega$, see section 3.5, if the damping functions, Eqs. 65, 67 and 69, are set equal to 1, $9/100$ and $5/9$, respectively.

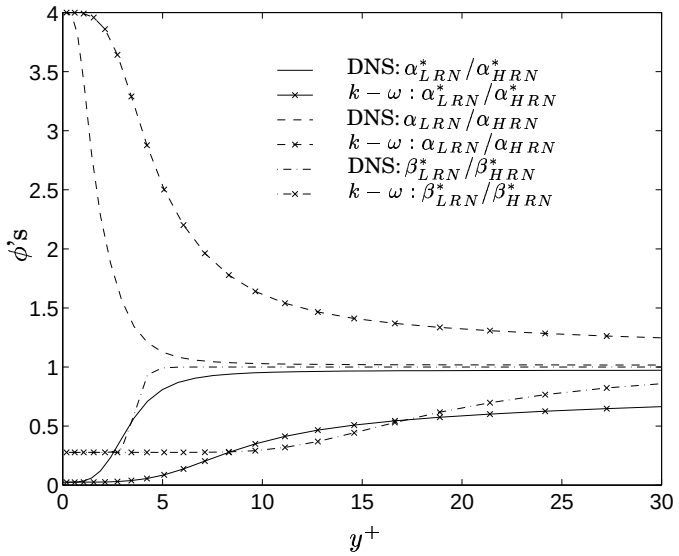

Figure 10: Damping functions in Wilcox $k-\omega$ models. Channel flow, DNS-data, [25].

4.1.1 The damping functions

The near-wall behaviour of the three important constants α^*, β^* and α are shown in Fig. 10. The introduction of the wall viscous effects, via the damping functions in LRN-model can observed in the figure. The results are based on both a priori DNS-data, $Re_\tau = 395$ [25], and also on a computation made using the $k-\omega$ model.

As can be seen in the figure the damping functions are most effective in the viscous sub-layer and in the inner part of the buffer layer, while the HRN and LRN $k-\omega$ formulations become similar in the inertial sub-layer.

In the limit of $Re_t = 0$, i.e. at the wall, the coefficients for the LRN and HRN formulation give:

	LRN	HRN	LRN/HRN
$\alpha^*_{y\to 0}$	0.025	1	0.025
$\beta^*_{y\to 0}$	0.025	0.09	0.28
$\alpha_{y\to 0}$	2.22	0.55	4
$\beta_{y\to 0}$	0.075	0.075	1
$(\alpha\alpha^*)_{y\to 0}$	0.055	0.55	0.1

Thus, in the near-wall region, the production terms (first terms on the RHS of Eqs. 66 and 68) of the LRN $k-\omega$ model are reduced as compared with the HRN $k-\omega$ model, through the reduced eddy-viscosity, ν_t, via α^*. In addition, the dissipation term (the second term on the RHS) of the k-equation, Eq. 66, is also reduced, through β^*.

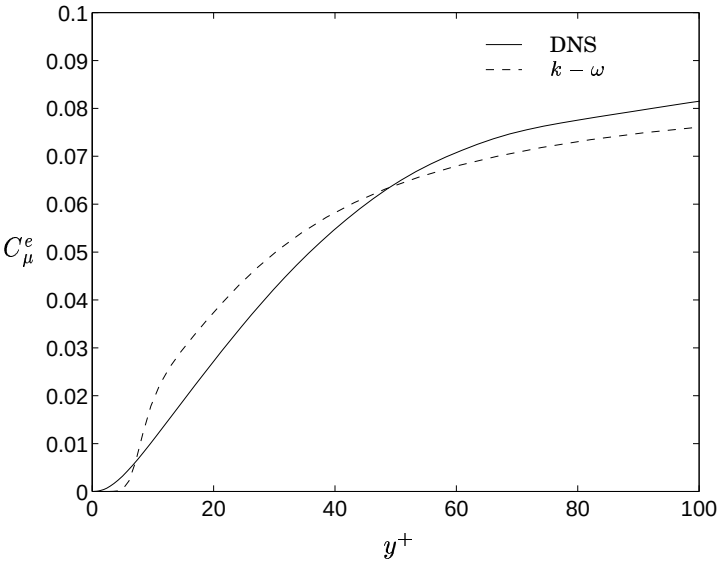

Figure 11: C^e_μ-coefficient, LRN $k-\omega$ and DNS $Re_\tau = 395$ [25].

4.1.2 C_μ modification, α^*

The most important damping function is the damping of the turbulence kinetic viscosity, ν_t. This is done by adding a damping function to C_μ, which reduces C_μ to an effective C^e_μ according to:

$$C^e_\mu = f_\mu C_\mu = \left(\frac{\overline{u'v'}}{k}\right)^2 \tag{70}$$

Measurements and DNS show that the assumed relation of $\overline{u'v'}/k = 0.3$ is valid only in the inertial sub-layer. The ratio is reduced in the near-wall region, as shown in Fig. 9. For a $k-\varepsilon$ model the effective C_μ is computed as:

$$C^e_\mu = \frac{\nu_t \varepsilon}{k^2} \tag{71}$$

Using a $k-\omega$ formulation, both ν_t and ε in the relation must be substituted with the appropriate definitions. In the case of the LRN $k-\omega$ turbulence model, ε is equal to

$\beta^* k\omega$, while the turbulent viscosity is defined as in Eq. 64. The effective C_μ^e thus becomes:

$$C_\mu^e = \alpha^* \beta^* \tag{72}$$

where α^* and the second part (non 0.09) of β^* perform the role of the damping function, f_μ, found in $k-\varepsilon$ turbulence models. Any deviation from the correct C_μ^e is primarily modelled with the damping function, α^*. Note however that the turbulence equations are strongly coupled, and thus a change to the damping functions in either k or ω would also require a modification of α^*.

The variation in the computed C_μ^e using the LRN $k-\omega$ is compared with DNS-data in Fig. 11. The agreement is good, especially as compared to other models, see e.g. Patel *et al.* [26].

4.1.3 Production-to-dissipation rate

Another important parameter in a turbulence model is the correct modelling of the production-to-dissipation rate, P_k/ε. By comparing the HRN and LRN formulation of the $k-\omega$ model, it is possible to show the effect these damping functions have on the production-to-dissipation ratio.

From Eq. 66, and assuming 1D flow, the production-to-dissipation rate is:

$$\begin{aligned}\frac{P_k}{\varepsilon} &= \alpha^* \frac{k}{\omega} \left(\frac{dU}{dy}\right)^2 \Bigg/ \beta^* k\omega \approx \\ &\approx \alpha^* \left(\frac{u_\tau}{\kappa y}\right)^2 \Bigg/ \beta^* \left(\frac{u_\tau}{\sqrt{\beta_0^*}\kappa y}\right)^2 = \\ &= \frac{(\alpha_0^* + Re_t/R_k)}{(1+Re_t/R_k)} \frac{\left[1+(Re_t/Re_\beta)^4\right]}{\left[5/18+(Re_t/R_\beta)^4\right]}\end{aligned} \tag{73}$$

where β_o^* is the value of β^* in the logarithmic region, $\beta^* = 0.09$. The log-laws, Eqs. 46 and 48, were used in the relations for dU/dy and ω, respectively. The approximate identity is correct only in the inertial sub-layer for which the log-laws are valid. In the near-wall region, $y^+ < 10$, the above relation may only be used qualitatively. The *a priori* computed production-to-dissipation ratios for the HRN and LRN formulation are compared with DNS-data in Fig. 12.

The LRN formulation, similar to the DNS-data, increases the production in the buffer layer, which results in a 50% higher peak of k for the LRN-model as compared with the HRN-model. Slightly dependent on the Reynolds number, DNS-data give the peak of turbulent kinetic energy at around $y^+ = 15$, close to the maxima of the P_k/ε-ratio given in Fig. 12.

4.1.4 Rationale behind the α and β^* coefficients

As was previously shown, the damping function, α^*, was introduced to reduce the turbulence viscosity in the near-wall region. This also effectively reduces the production terms in the k- and ω-equations. In order to predict the same level of turbulence, the dissipation term in the k-equation must also be reduced. This can be arranged in three different ways:

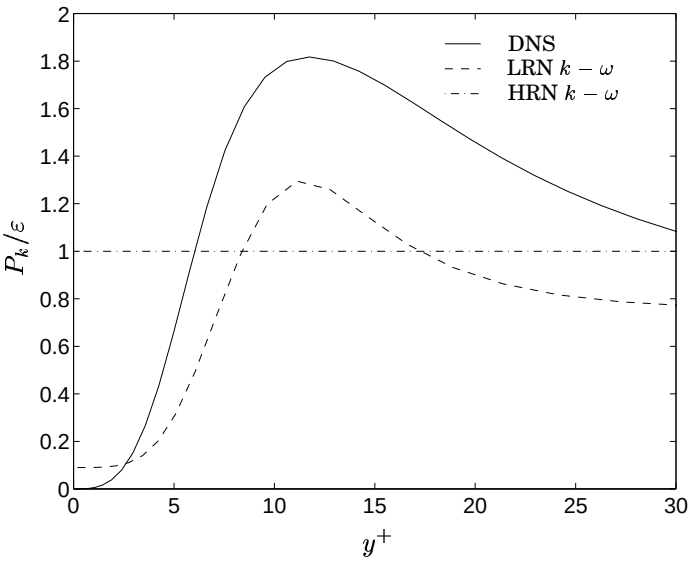

Figure 12: Production-to-dissipation ratio, HRN and LRN formulation of the $k-\omega$. Channel flow, DNS-data at $Re_\tau = 395$.

- Decrease the coefficient for the dissipation term in the k-equation.
- Increase the coefficient for the production term in the secondary equation (ε or ω).
- Decrease the coefficient for the destruction term in the secondary equation.

The last method is commonly employed in the $k-\varepsilon$ models. By properly balancing the dissipation rate equation, a desirable level of k is predicted that matches the computed ε. Because the production of dissipation is automatically decreased through the reduction of ν_t, the simplest correction is to reduce the destruction term in the dissipation rate equation. This is usually done in a $k-\varepsilon$ model by introducing a damping function f_2, see Patel *et al.* [26].

There is more to the damping functions than balancing the equations, however. As previously discussed, it is also important to predict an accurate production-to-dissipation ratio, which puts an additional demand on the actual values of k and $\varepsilon = \beta^*\omega k$. In a $k-\omega$ model, where the dissipation term is a function of both ω and k, it is unrealistic to believe that merely modifying the ω-equation would yield a correct P_k/ε, as well as a correct level of k. Hence, apart from modifying the specific dissipation rate equation, the dissipation term in the k-equation is also modified. In the LRN $k-\omega$ model these two aspects are accomplished through both an increase of production of ω (increasing α), and a reduction of the dissipation term in the k-equation (decreasing β^*). Note however that, contrary to the $k-\varepsilon$ model, the destruction term in the secondary equation (ε, ω) is unchanged.

Considering Patel *et al.* [26], it seems likely that the minimum number of damping functions required for an Eddy-Viscosity Model (EVM) to correctly predict the turbulent kinetic energy, k, in the near-wall region is three. In that paper the only model that accurately reproduces the profile of k is the Lam-Bremhorst [21] $k-\varepsilon$ model,

which is one of only two models tested employing three damping functions.

4.2 HRN-models: Wall Functions

The rationale behind wall function is the reduced computational requirement and the increase numerical stability and convergence speed. By adopting a mesh, where the first interior node is located in the inertial sub-layer, it is possible to use the law-of-the-wall to specify the boundary condition for the dependent variables u, k and ω.

4.2.1 Standard wall functions

In its simplest form, the logarithmic laws, Eqs. 46, 47, 48 are directly applied to the first interior node. These wall functions are here referred to as the standard wall function method. The three steps involved in a CFD-code would then be:

- Solve the momentum equation with a modified wall friction, either through an added source term or via a modified effective viscosity.
- Set k at the first node iteratively with the use of the law-of-the-wall.
- Set ω with k.

In a turbulent boundary layer, the strongest velocity gradient is found close to the wall. With a wall-function based turbulence model, which utilises a relatively coarse mesh, it is impossible to resolve these near-wall gradients. The predicted wall friction would thus be largely in error if a modification is not introduced:

$$\tau_w \equiv \mu \left.\frac{\partial U}{\partial y}\right|_w > \mu \frac{\Delta U}{\Delta y} = \mu \frac{U_p}{y_p} \tag{74}$$

where the subscript p is used for the first interior node. The necessary modification could either be made through

(i) an added source term simulating the correct wall friction or

(ii) a modified viscosity, an effective viscosity, μ_e, that ensures the correct friction even though the velocity gradient is erroneous.

Through the law-of-the-wall:

$$\frac{U}{u_\tau} = \frac{1}{\kappa} \ln(E y^+) \tag{75}$$

the wall friction is computed as

$$\tau_w = \frac{\rho u_\tau U \kappa}{\ln(E y^+)} \tag{76}$$

with $\tau_w \equiv \rho u_\tau^2$.

For a wall function based model this can either be set directly using a source term, $S_u = \tau_w \cdot A$, or via a modified effective wall viscosity [10]:

$$\mu_e \frac{U_p}{y_p} = \tau_w = \frac{\rho u_\tau U_p \kappa}{\ln(E y_p^+)} \qquad \Rightarrow \; \mu_e = \frac{\rho u_\tau y_p \kappa}{\ln(E y_p^+)} \tag{77}$$

The turbulent kinetic energy is set in the first node by iteratively computing the friction velocity from the law-of-the-wall. This iterative process is needed because u_τ appears implicitly in the log-law. Initially u_τ is set from Eq. 47, as $u_\tau = \beta^{*1/4}\sqrt{k_p}$. Using this relation, a new u_τ is found from the log-law:

$$u_\tau = \frac{U_p \kappa}{\ln(E y_p^+)} \qquad \text{where} \quad y_p^+ = \frac{y_p u_\tau}{\nu} \tag{78}$$

The new value is then used to compute y_p^+ and re-fed into the u_τ expression. This process is repeated until convergence, with the turbulent kinetic energy finally set as:

$$k_p = \frac{u_\tau^2}{\sqrt{\beta^*}} \tag{79}$$

For the specific dissipation rate, ω, the friction velocity, u_τ, is substituted by the relation for k in the log-law as:

$$\omega_p = \frac{u_\tau}{\sqrt{\beta^*}\kappa y_p} = \frac{\beta^{*1/4}\sqrt{k_p}}{\sqrt{\beta^*}\kappa y_p} = \frac{\sqrt{k_p}}{\beta^{*1/4}\kappa y_p} \tag{80}$$

4.2.2 Launder-Spalding methodology

The standard wall function method is very limited in its usage. This is especially true for re-circulating flows, where the turbulent kinetic energy becomes zero in separating and re-attachment points, where, by definition, u_τ is zero. This singular behaviour severely deteriorates the predictions of, for instance, heat transfer in rib-roughened channels. Launder-Spalding [24] proposed a modification to the standard wall function method that involves the following steps:

- Solve the momentum equation with a modified wall viscosity.
- Solve the turbulent kinetic energy, with modified integrated production and dissipation terms.
- Set ε using the predicted k.

The same reason and method of specifying the wall viscosity as for the standard wall functions apply in this case. However, instead of using u_τ in the log-law, the identity $u_\tau = C_\mu^{1/4}\sqrt{k}$ is utilised:

$$\mu_e = \frac{\rho C_\mu^{1/4}\sqrt{k_p} y_p \kappa}{\ln(E y_p^*)} \tag{81}$$

where y_p^* is defined with k as:

$$y_p^* = \frac{y C_\mu^{1/4}\sqrt{k}}{\nu} \tag{82}$$

In the k-equation, the integrated production term is defined from (1D):

$$\int \rho P_k dy \equiv \int \tau_t \frac{\partial U}{\partial y} dy \tag{83}$$

In the inertial sub-layer the laminar shear stress, $\tau_l \equiv \mu \partial U/\partial y$, is negligible and, by assuming that the shear

stress is constant, the turbulent shear stress, τ_t, is equal to the wall shear stress:

$$\begin{aligned} &\tau = \tau_l + \tau_t \qquad \{\tau = \tau_w,\, \tau_l = 0\} \;\Rightarrow \\ &\tau_t = \tau_w \end{aligned} \tag{84}$$

The accuracy of this assumption is shown in Fig. 1. The production can be set using the law-of-the-wall:

$$\begin{aligned} \int \rho P_k dy = \int \tau_w \frac{\partial U}{\partial y} dy = \tau_w \Delta U = \mu_e \frac{U_p}{y_p} \Delta U = \\ = \{\text{Eq. } 81\} = \frac{\rho C_\mu^{1/4} \sqrt{k} U_p \kappa}{\ln(E y_p^*)} \Delta U \end{aligned} \tag{85}$$

The integration of $\int \tau_w \left(\partial U / \partial y\right) dy$ is equal to $\tau_w \Delta U$, since τ_w is constant.

To set the value for the dissipation rate, production is assumed to be equal to dissipation:

$$P_k = \varepsilon \tag{86}$$

The production can be re-written as:

$$P_k = -\overline{u'v'} \frac{\partial U}{\partial y} = u_\tau^2 \frac{u_\tau}{\kappa y} \tag{87}$$

where the constant shear stress approximation, Eq. 54, $\tau_{xy} = -\rho \overline{u'v'} = \rho u_\tau^2$, and the law-of-the-wall, $\partial U / \partial y = u_\tau / (\kappa y)$, were used. Integrating the dissipation rate between the wall and the edge of the first cell, Δy, yields:

$$\int_0^{\Delta y} \varepsilon dy = \int_0^{\Delta y} \frac{u_\tau^3}{\kappa y} dy = \frac{u_\tau^3}{\kappa} \left[\ln(\Delta y) - \ln(0)\right] \tag{88}$$

The mathematical singularity at the wall of this equation ($\ln(0)$) necessitates re-consideration. The shortcoming of the above derivation is the assumption that the law-of-the-wall is valid all the way from the wall, which is erroneous.

However, by choosing a different relation for the integrated ε, other approximations could be found. The integrated velocity gradient in the production term can, according to the mean value theorem, be re-written as:

$$\int_0^{\Delta y} \frac{\partial U}{\partial y} dy = \Delta y \frac{\partial U}{\partial y} \tag{89}$$

for a certain value of $\partial U / \partial y$. Approximating the velocity gradient with discrete values, $\Delta U / \Delta y$, and, assuming that this value could be established in the inertial sub-layer, the velocity gradient could be re-written with the help of the law-of-the-wall:

$$\frac{\partial U}{\partial y} \approx \frac{\Delta U}{\Delta y} = \frac{u_\tau}{\kappa \Delta y} \ln(E y^*) \tag{90}$$

Hence the integrated dissipation rate can also be written as:

$$\begin{aligned} \int_0^{\Delta y} \varepsilon dy = \int_0^{\Delta y} P_k dy = \{\text{Eq. } 87\} = \int_0^{\Delta y} -\overline{u'v'} \frac{\partial U}{\partial y} dy = \\ = \{\text{Eq. } 90\} = u_\tau^2 \Delta y \frac{u_\tau}{\kappa \Delta y} \ln(E y^*) = \frac{u_\tau^3}{\kappa} \ln(E y^*) \end{aligned} \tag{91}$$

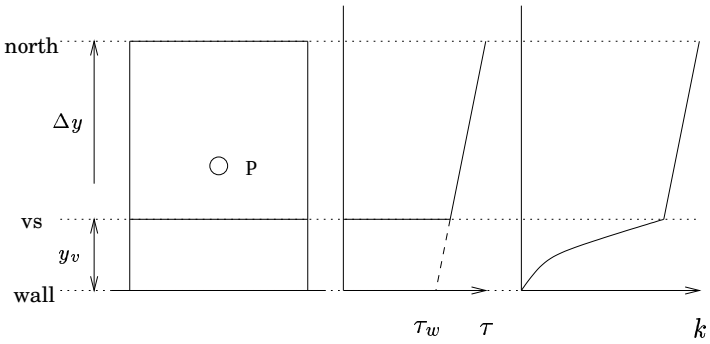

Figure 13: Assumed variation of variables in the first computational node, Chieng-Launder model. vs=edge of viscous sub-layer.

Comparing the two formulations, Eqs. 88 and 91, gives:

$$\underbrace{\ln(\Delta y) - \ln(0)}_{\text{Eq. } 88} \stackrel{?}{=} \underbrace{\ln(E y^*)}_{\text{Eq. } 91} \tag{92}$$

The latter formulation is used in the Launder-Spalding model, with the integrated dissipation rate in the k-equation set as:

$$\int \varepsilon dy = \frac{C_\mu^{3/4} k_p^{3/2}}{\kappa} \ln(E y_p^*) \tag{93}$$

where u_τ^3 in Eq. 91 has been substituted by $C_\mu^{3/4} k^{3/2}$. Note that in [24], C_μ is used rather than $C_\mu^{3/4}$, although this is most probably a typographical error.

The dissipation rate equation is not solved for the first interior node, and ε is instead fixed according to:

$$\varepsilon = \frac{u_\tau^3}{\kappa y} = \frac{C_\mu^{3/4} k_p^{3/2}}{\kappa y_p} \tag{94}$$

which is a direct consequence of substituting the friction velocity with the log-law for turbulent kinetic energy, $u_\tau = C_\mu^{1/4} \sqrt{k}$, into Eq. 86.

4.2.3 Improvements of the near-wall representation, Chieng-Launder model

It is evident from the above derivation that there is room for improvement in the Launder-Spalding model, especially in its representation of the near-wall region. Chieng and Launder [7] enhanced the model by introducing a more complete model of the near-wall turbulence. They argued that there exists two distinct regions, the viscous sub-layer and the inertial sub-layer, which have different turbulent structure. The partition line between these regions is defined by a viscous sub-layer Reynolds number:

$$Re_v = \frac{y_v \sqrt{k_v}}{\nu} \tag{95}$$

The near-wall variation in the variables assumed in the Chieng and Launder model is shown in Fig. 13.

The turbulent shear stress is zero for $y < y_v$ and is linearly interpolated between the wall friction and the

shear stress at the edge of the cell for $y > y_v$:

$$\begin{aligned} \tau_t &= 0 && y < y_v \\ \tau_t &= \tau_w + (\tau_n - \tau_w)\frac{y}{y_n} && y > y_v \end{aligned} \tag{96}$$

where subscripts n and w are used for the value at the north edge of the cell and at the wall, respectively.

The turbulent kinetic energy is approximated as:

$$\begin{aligned} k &= k_v \left(\frac{y}{y_v}\right)^2 && y < y_v \\ k &= k_v + y\frac{k_n - k_v}{y_n - y_v} && y > y_v \end{aligned} \tag{97}$$

The dissipation rate is approximated in the region below y_v by the viscous sub-layer approximation used in numerous $k-\varepsilon$ turbulence models, e.g. Jones and Launder [15], while the log-law is used for $y > y_v$:

$$\begin{aligned} \varepsilon &= 2\nu\left(\frac{\partial\sqrt{k}}{\partial y}\right)^2 = \frac{2\nu k_v}{y_v^2} && y < y_v \\ \varepsilon &= \frac{C_\mu^{3/4} k_p^{3/2}}{\kappa y_p} && y > y_v \end{aligned} \tag{98}$$

The turbulent kinetic energy gradient in the first relation is approximated using the previously assumed variation in k in the viscous sub-layer, i.e. $k \sim y^2$.

Because the finite volume method commonly applied, and the strong variation in these quantities in the near-wall region, it is advantageous to use integrated relations in the first computational cell. The resulting terms are then incorporated into the k-equation, which is subsequently solved. In additional and identical to the Launder-Spalding model, the wall friction is corrected and the dissipation rate set. However, before continuing with the integration of k and ε, it is proper to define the location of the viscous sub-layer. In the Chieng-Launder model, y_v is deduced from the assumption that the sub-layer Reynolds number is constant and equal to 20, and hence:

$$y_v = \frac{20\nu}{\sqrt{k_v}} \tag{99}$$

However, since k_v is unknown, the problem is not closed. k_v is approximated by extrapolating the slope of k from the computed k's in the two first near wall nodes. It should be noted however that this methodology is not numerically satisfying. It can be shown using DNS-data that $Re_v = 20$ is found at $y^+ = 11.5$. The profile of k around this value can be seen in Figs. 4 and 5. The maxima of k is found at $y^+ = 15$. Thus the computed slope of k using nodes 1 and 2, located at say $y^+ = 30$ and $y^+ = 100$ becomes negative, which may be of concern in terms of numerical stability.

In the Chieng-Launder model, the common practise of estimating the friction velocity with the turbulent kinetic energy is taken one step further, with the law-of-the-wall modified as:

$$\frac{U\sqrt{k_v}}{\tau_w/\rho} = \frac{1}{\kappa^*}\ln\left(E^*\frac{y\sqrt{k_v}}{\nu}\right) \tag{100}$$

where the new constants, $\kappa^* = 0.23$ and $E^* = 5.0$, are related to the standard values, through the identities: $\kappa^* = \kappa C_\mu^{1/4}$ and $E^* = EC_\mu^{1/4}$. For local equilibrium flow, $k = u_\tau^2/\sqrt{C_\mu}$, and with the above identities, the modified law-of-the-wall reduces to the standard formulation.

The integrated production following the same grounds as for the Launder-Spalding model yields (1D):

$$\begin{aligned} &\int \rho P_k dy = \\ &= \underbrace{\int_0^{y_v} \tau_t \frac{\partial U}{\partial y} dy}_{\to 0} + \int_{y_v}^{y_n} \left[\tau_w + (\tau_n - \tau_w)\frac{y}{y_n}\right]\frac{\partial U}{\partial y} dy \end{aligned} \tag{101}$$

The first part is identical zero, since the turbulent shear stress is assumed to be zero in the viscous sub-layer. The second part is split into two, where the first part is easily integrated:

$$\int_{y_v}^{y_n} \tau_w \frac{\partial U}{\partial y} dy = \tau_w (U_n - U_v) \tag{102}$$

In the second part, the velocity gradient is re-written using the law-of-the-wall:

$$\begin{aligned} &\int_{y_v}^{y_n} \left[(\tau_n - \tau_w)\frac{y}{y_n}\right]\frac{\partial U}{\partial y} dy = \\ &\quad = \int_{y_v}^{y_n} \left[(\tau_n - \tau_w)\frac{y}{y_n}\right]\frac{\tau_w/\rho}{\sqrt{k_v}\kappa^* y} dy = \\ &\quad = \frac{\tau_w(\tau_n - \tau_w)}{\rho\sqrt{k_v}\kappa^* y_n}(y_n - y_v) \end{aligned} \tag{103}$$

The wall friction, τ_w, used in these relations is deduced from the above modified law-of-the-wall, Eq. 100.

The integration of the dissipation term is given as:

$$\begin{aligned} &\int \varepsilon dy = 2\frac{k_v^{3/2}}{Re_v} + \\ &\quad + \frac{1}{C_l}\left[\frac{2}{3}(k_n^{3/2} - k_v^{3/2}) + 2a(k_n^{1/2} - k_v^{1/2}) + \lambda\right] \end{aligned} \tag{104}$$

where $C_l = 2.55$. The constant, λ, depends on the turbulent kinetic energy via variable a:

$$\begin{aligned} \lambda =& a^{3/2}\log\left[\frac{(\sqrt{k_n} - \sqrt{a})/(\sqrt{k_n} + \sqrt{a})}{(\sqrt{k_v} - \sqrt{a})(\sqrt{k_v} + \sqrt{a})}\right] \quad a > 0 \\ \lambda =& 2(-a)^{3/2}\left[\tan^{-1}\frac{\sqrt{k_n}}{\sqrt{-a}} - \tan^{-1}\frac{\sqrt{k_v}}{\sqrt{-a}}\right] \quad a < 0 \end{aligned} \tag{105}$$

with

$$a = k_p - \frac{(k_p - k_n)}{(y_p - y_n)} y_p \tag{106}$$

4.2.4 Modification to the Chieng-Launder model

The assumption of $Re_v = 20$ is not valid for all types of flows. Using DNS-data on fully developed channel flows, $Re_v = 20$ is equivalent to $y^+ = 11.5$, which is the location of the cross-over of the linear law, $U^+ = y^+$, and the log-law, $U^+ = 1/\kappa\ln(Ey^+)$. Thus, for equilibrium flows,

$Re_v = 20$ is a good partition value, since the two formulations become a laminar and a turbulent approximation, respectively.

However, in a subsequently paper by Johnson and Launder [14], it was found that the heat transfer prediction could be improved by letting the viscous sub-layer thickness, i.e. the sub-layer Reynolds number, vary according to the turbulence level:

$$Re_v = Re_{v0} - CRe_v \frac{k_v - k_w}{k_v} \tag{107}$$

where $C = 0.5C_\mu C_l$, and k_w is the linear extrapolated turbulent kinetic energy at the wall.

Ciofalo and Collins [8] used an approach however where they proposed to let the sub-layer thickness vary, dependent on the turbulence intensity.

4.2.5 Extensions to the Chieng-Launder model

Amano *et al.* ([2], [3]) devised two different models based on the same zonal principle as the Chieng-Launder model. In both models, the dissipation rate equation is solved using the layered approach rather than allowing it to be set as in the Chieng-Launder model. The results were only marginally improved however, and hence the two-layered approach was extended in the second model to a three-layered version. Here the parameters, τ, k, ε were allowed to vary in accordance with measured data for the viscous sub-layer, the buffer layer and the inertial sub-layer.

4.3 New Model: Blending Integrating and Wall Function Boundary Conditions

The physical treatment improved, w hen progressing from the Launder-Spalding model to the more advanced models, although at the expense of increased numerical complexity. The modifications by Johnson and Launder [14] and Ciofalo and Collins [8] showed that the improvements with the zonal approach were not particularly great if a variable sub-layer thickness was not included. The further refinement by Amano *et al.* enhanced the predictions only marginally, with a significantly increased complexity.

Thus, here, instead of further optimising the layered models, a new strategy will be adopted.

Two main problems with wall-functions must be addressed to make such an effort worthwhile:

- The negligence of the physics in the viscous sublayer,
- The necessity of locating the first computational node in the inertial sub-layer

The first problem has been discussed in numerous papers, see e.g. Launder [22]. The conclusion made in these studies is that the standard wall function formulation (HRN-models) are indisputably inferior to the integrating formulation (LRN-models). This is particularly true for non-equilibrium flows, where it is of critical importance to include the variation found in the viscous sub-layer in order to accurately predict the wall friction and heat transfer. To be able to significantly improve the results, it is necessary to mimic the LRN method of resolving the viscous sub-layer, especially in non-equilibrium regions. Thus the wall function approach of bridging the viscous sub-layer seems unattainable, apart from regions in which the flow is in equilibrium. Hence the only possible path to reducing the computational demands and maintain accuracy would be a turbulence model that adopts itself to the flow, employing a LRN type model where necessary and switching to a HRN type model otherwise. While such artificial intelligence may sound incredible it is possible to achieve it through a smartly devised model.

The second problem is associated with the underlying physics of the wall functions, i.e. the law-of-the-wall. When employing wall function, it is necessary to apply the first computational node in the inertial sub-layer. This fact is less of a problem in equilibrium flow but it is accentuated in regions of flow separation[2], where the wall shear stress and hence y^+ decreases. For these regions, the size of the first cell must be enlarged to ensure that the cell node is kept within the logarithmic region. Hence the mesh generation becomes a delicate business using wall functions for re-circulating flows.

Both of the above explained problems are solved with the two-layer Chieng-Launder model. The CL-model, however gives rise to additional complexity. Through prolonged mathematical operations the viscous sublayer and the inertial sub-layer are modelled simultaneously, although the author encountered numerical difficulties using this approach. If the two regionscould be separate mathematically, a numerically simpler and more robust wall function could be constructed.

Such a turbulence model will be presented here. A less complete derivation is given in Bredberg *et al.* [6], where predictions of heat transfer in rib-roughened channels are included. The reader is referred to the paper for a discussion of the accuracy and for comparisons between the model and other turbulence models.

Dependent on some flow quantity, the model will either employ a wall function or use the integrating method as a wall boundary condition, and hence greatly simplify the numerical scheme as compared to the Chieng-Launder model. The new model will, like the wall function, approach reducing the computational demand – by coarsening the mesh, when possible, and still be able to produce accurate results through the use of the LRN part of the model, when necessary. The physical consequence of separating and re-circulating regions can actually be utilised with such an adopting turbulence model. In non-equilibrium nodes where the physics reduces the y^+ value, the hybrid model automatically switches to the LRN mode, producing accurate results even for a relative coarse mesh. Thus even a uniform mesh could be sufficient for complex re-circulating flow, and, as a result, reduces the workload of mesh-generation substantially.

[2]Although the log-law in itself is rather questionable in such circumstances.

4.3.1 Blending function

The critical part of a hybrid turbulence model is the construction of the function that effectively changes the model into either LRN or HRN mode. It is numerically undesirable to adopt a function that abruptly switches between the two different modes. It is also physically questionable, because the flow is only strictly laminar in the immediate near-wall region – enabling an LRN model to be used – while only in the inertial sub-layer can the flow be treated as fully turbulent. The latter is of course a requirement for using a wall function-based HRN-model, see Fig. 1. In the buffer layer it is thus most appropriate to employ a smoothing function that blends the two formulation together. One of the simplest mathematical functions that accomplishes this is the exponential function, which can be designed to operate from 0 to 1 dependent on some flow quantity. On the grounds of the above discussion, it would be most beneficial to base the exponential function on y^+. However owing to numerical issues, it is disadvantageous to include any wall distance, and hence the blending function is instead constructed using the turbulent Reynolds number, $Re_t = \nu_t/\nu$ as:

$$f = exp^{-Re_t/C} \tag{108}$$

where C is a tunable constant.

The model is then constructed to linearly combine the LRN and HRN formulations using this blending function. Since $Re_t = 0$, and hence $f = 1$ at the wall, f is multiplied with the LRN part and $(1 - f)$ is multiplied with the HRN part:

$$\phi_{TOT} = f\phi_{LRN} + (1 - f)\phi_{HRN} \tag{109}$$

where ϕ is some turbulent quantity. The LRN and HRN parts needed in this model are treated separately below.

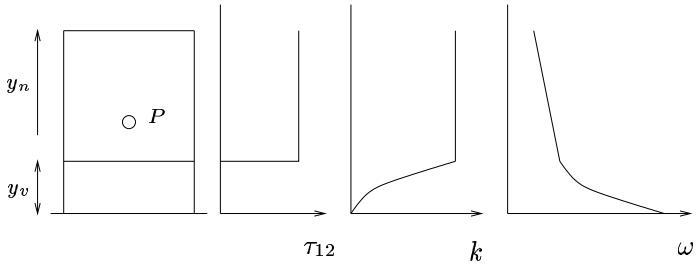

Figure 14: Assumed variation of variables first interior node, new model.

4.3.2 HRN part: Simplified Chieng-Launder model applied to a $k-\omega$-type turbulence model

The logarithmic equations based on u_τ, Eqs. 25 and 41 are unsuitable in separated flows. This applies especially for heat transfer since the predicted Nusselt number becomes zero in separation and re-attachment points using these equations. In contrast, experiments indicate a maximum level of heat transfer at or in the vicinity of these points (Launder [23]). Substituting u_τ with $\sqrt{k}$ improves predictions for non-equilibrium flows. This is utilised by the Launder-Spalding model and subsequent models. In addition the HRN part of the new model assumes a variation of the near-wall turbulence similar to what is done in the Chieng and Launder model. However, since the viscous sub-layer is treated separately from the HRN part in the new model, a simplified model is sufficient here. The model is also adopted to a $k-\omega$-type turbulence model.

The assumed variation of the dependent variables for this model are shown in Fig. 14. Both the turbulent kinetic energy and the shear stress have lost their linear variation in the inertial sub-layer, as compared to the Chieng-Launder model. This of course simplifies the treatment immensely. The specific dissipation is assumed to vary either according to the log-law, $1/y$, or the linear-law, $1/y^2$.

As was stated above, only the region above the viscous sub-layer is of interest in this section. The integrated production of turbulent kinetic energy in the HRN region, i.e. from $y_v < y < y_n$, is found as:

$$\int_{y_v}^{y_n} \rho P_k dy = \int_{y_v}^{y_n} \rho\overline{u'v'}\frac{\partial U}{\partial y}dy \approx \tau_w(U_n - U_v) \tag{110}$$

The last identity can be used only if it can be assumed that the shear stress is constant and that the laminar shear stress is negligible in the inertial sub-layer, see Fig. 1 and the discussion in connection with Eq. 84.

The wall shear stress in the new model is set similar to the Chieng-Launder model (see Eq. 100) as:

$$\tau_w = \frac{\kappa^*\rho U_p\sqrt{k_v}}{\ln(E^* y_p\sqrt{k_v}/\nu)} \tag{111}$$

where κ^* and E^* are set to 0.22 and 4.5, respectively, in order to comply with the equilibrium values of the $k-\omega$ turbulence model. The *a priori* result using this equation is compared with the turbulent shear stress predicted using the LRN $k-\omega$ model in Fig. 15. Note that

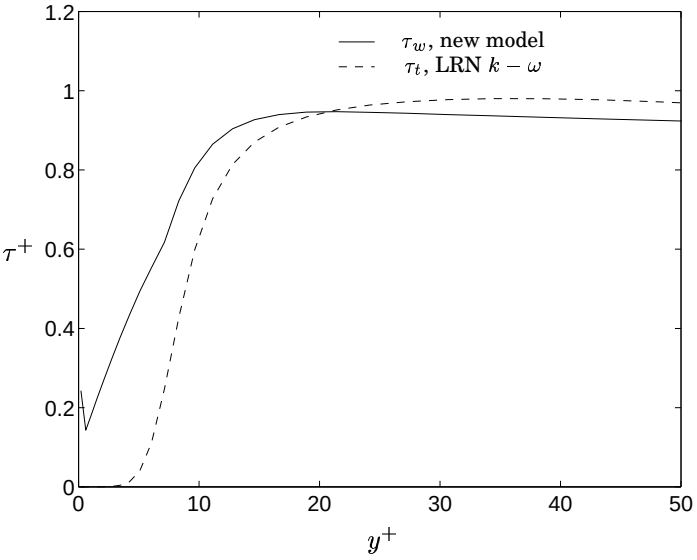

Figure 15: The accuracy of the assumption, $\tau_w \approx \tau_t$. Channel flow.

the turbulent production is negligible in the near-wall

region; hence any discrepancy comparing to the Chieng-Launder model is a consequence of the simplistically assumed variation in the turbulent shear stress. At this moment it may perhaps be of interest to compare the turbulent shear stress given by DNS-data, Fig. 1, with the assumed variations of the two models. The assumption of a constant turbulent shear stress beyond y_v (new model) is perhaps not any worse than the linear variation from the wall shear to edge of the cell in the Chieng-Launder model. Note especially in Fig. 1 that the (laminar) wall shear is higher than any given turbulent shear, and hence the linear **increase** in the turbulent shear from the wall shear is **not** physically founded.

The integrated dissipation rate of the turbulent kinetic energy is based on the logarithmic law, Eq. 48:

$$\begin{aligned}\int_{y_v}^{y_n} \varepsilon dy = \int_{y_v}^{y_n} \beta^* \omega k dy = \int_{y_v}^{y_n} \beta^* \frac{\sqrt{k}}{\beta^{*1/4}\kappa y} k dy = \\ = \frac{\beta^{*3/4} k_p^{3/2}}{\kappa} \ln\left(\frac{y_n}{y_v}\right)\end{aligned} \tag{112}$$

where k was assumed constant.

Contrary to the Chieng-Launder model, the dissipation rate is not set using the log-law. Rather, the mean integrated value from the log-law is used:

$$\begin{aligned}\overline{\omega}_{v-n} = \frac{1}{y_n - y_v} \int_{y_v}^{y_n} \frac{\sqrt{k_p}}{\beta^{*1/4}\kappa y} dy = \\ = \frac{\sqrt{k_p}\ln(y_n/y_v)}{\beta^{*1/4}\kappa(y_n - y_v)}\end{aligned} \tag{113}$$

4.3.3 LRN part: Standard $k-\omega$

The LRN part of the model is identical to the Wilcox $k-\omega$ [34] (HRN) turbulence model. The model was shown in Eqs. 61- 63, and is shown again here for clarity:

$$\begin{aligned}\nu_t &= \frac{k}{\omega} \\ \frac{Dk}{D\tau} &= P_k - \beta^* k\omega + \frac{\partial}{\partial x_j}\left[(\nu + \sigma^*\nu_t)\frac{\partial k}{\partial x_j}\right] \\ \frac{D\omega}{D\tau} &= \gamma\frac{\omega}{k}P_k - \beta\omega^2 + \frac{\partial}{\partial x_j}\left[(\nu + \sigma\nu_t)\frac{\partial \omega}{\partial x_j}\right]\end{aligned}$$

with the production of turbulence computed as $P_k = 2\nu_t S_{ij}\partial U_i/\partial x_j$.

The model coefficients are:

$$\beta^* = 0.09,\ \beta = 3/40,\ \gamma = 5/9,\ \sigma^* = 1/2,\ \sigma = 1/2$$

The asymptotic boundary conditions applicable for the turbulent quantities are:

$$k_w \rightarrow 0 \tag{114}$$

$$\omega_w \rightarrow \frac{6\nu}{\beta y^2} \tag{115}$$

The latter relation is valid only for computational nodes within $y^+ < 2.5$ (Wilcox [36]). To establish a grid independent solution, 7-10 nodes are required in this range. Both requirements can however be eased, especially the latter, with negligible deterioration of the predictions, see e.g. Bredberg *et al.* [5], [4].

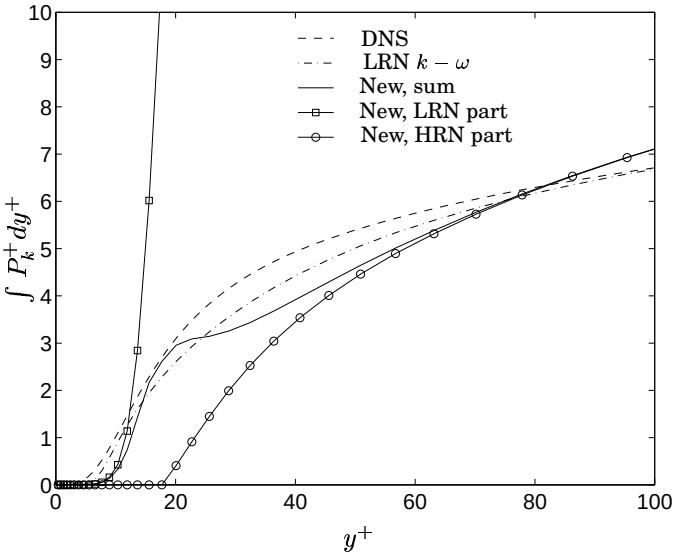

Figure 16: Integrated production term, k-equation. Channel flow, DNS-data, $Re_\tau = 395$ [25].

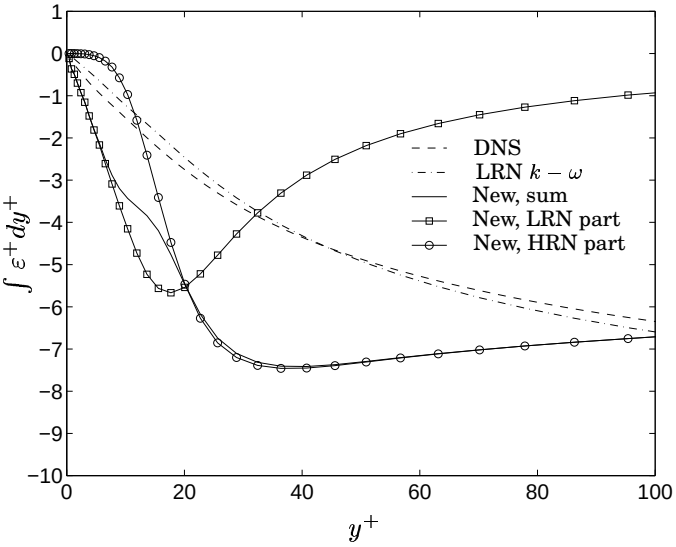

Figure 17: Integrated dissipation term, k-equation.

4.3.4 The blending $k-\omega$ turbulence model

The new blending $k-\omega$ turbulence model is summarised below and its performance is found in Bredberg *et al.* [6]. The production and dissipation terms in the turbulent kinetic energy equation are:

$$\int_0^{\Delta y} P_k dy = \tag{116}$$

$$\Delta y\left[f\nu_t\left(\frac{\partial U}{\partial y}\right)^2 + (1-f)\frac{\tau_w}{\rho}\frac{U_n - U_v}{y_n} + P'\right]$$

$$\int_0^{\Delta y} \beta^*\omega k dy = \tag{117}$$

$$\Delta y\left[f\beta^*\frac{6\nu}{\beta y_p^2}k_p + (1-f)\frac{\beta^{*3/4}k_p^{3/2}}{\kappa(y_n - y_v)}\ln\left(\frac{y_n}{y_v}\right)\right]$$

where P' is the contribution of the non-primary shear stress components ($\neq dU/dy$). The production term and the dissipation term are shown in Fig. 16 and Fig. 17, respectively.

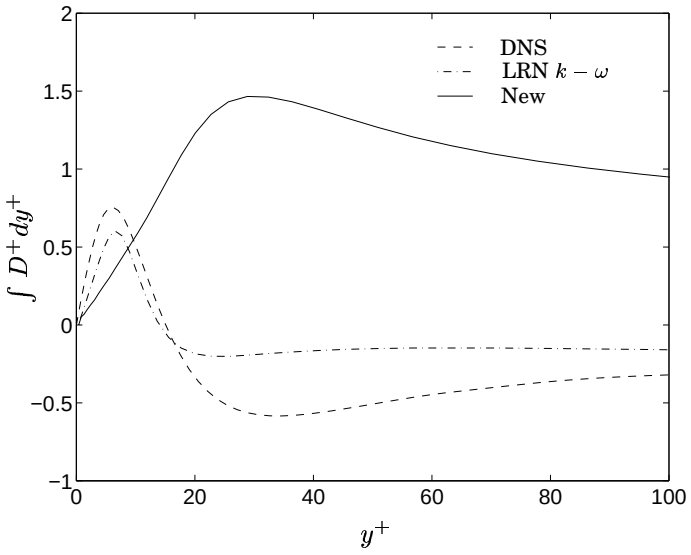

Figure 18: Integrated diffusion term, k-equation.

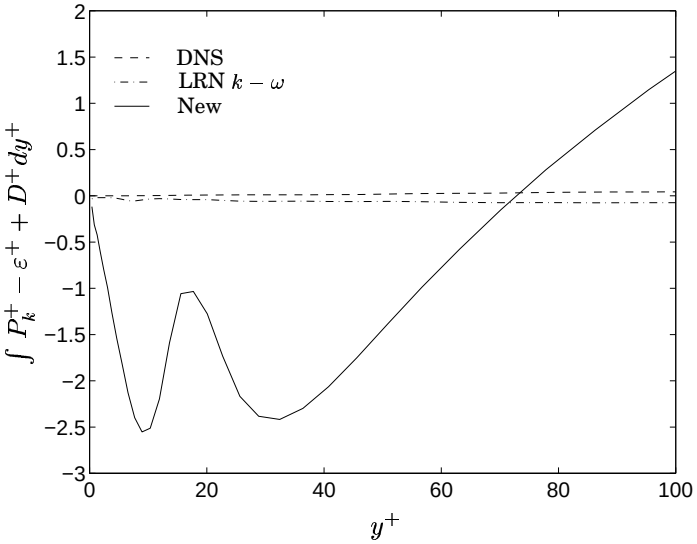

Figure 19: Sum of integrated source terms in k-equation.

The third source term on the RHS of the turbulent kinetic energy equation, Eq. 66, is the diffusion term, which is **not** modified in the present model, with the standard relation used. The accuracy using this simplistic model is shown in Fig. 18.

It is interesting to combine the three terms on the RHS of the turbulent kinetic energy equation in order to estimate its balance. This is done in Fig. 19. Both the DNS-data and the LRN $k-\omega$ mode yield perfect balance. The new model is not very well balanced, yielding a large negative source in the buffer layer and slowly increasing the value in the logarithmic region which yields a large positive source in the off-wall region. This latter fact may be the reason why the new model gives a fairly large discrepancy of the predicted k in the centre of a channel.

The specific dissipation in the first near-wall node is set as:

$$\omega_w = f\frac{6\nu}{\beta y_p^2} + (1-f)\frac{\sqrt{k_p}\ln(y_n/y_v)}{\beta^{*1/4}\kappa(y_n - y_v)} \tag{118}$$

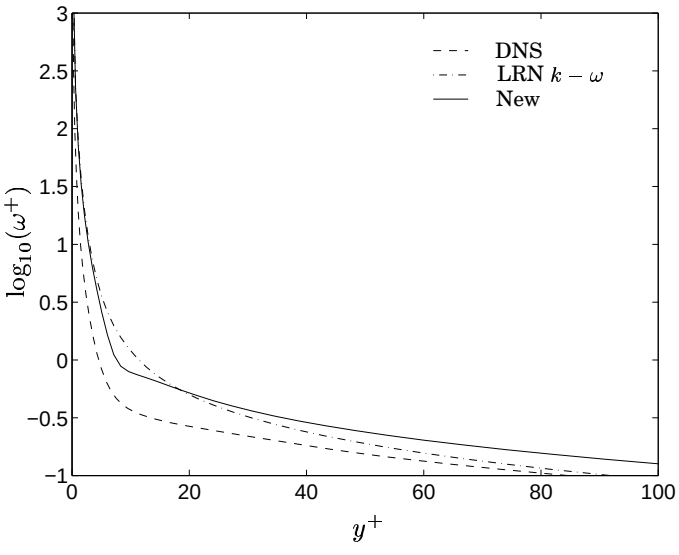

Figure 20: ω variation.

A comparison with DNS-data and the LRN $k-\omega$ model is shown in Fig. 20.

The wall viscosity is set as:

$$\nu_w = f\nu + (1-f)\left[\nu + \frac{\kappa^* y\sqrt{k_v}}{\ln(E^* y_p\sqrt{k_v}/\nu)}\right] \tag{119}$$

To close the model, the blending function, f (Eq. 108), and the viscous sub-layer values, y_v and k_v, must be defined. The viscous sub-layer thickness, y_v, is calculated using the definition of the viscous sub-layer Reynolds number and the assumed variation of the turbulent kinetic energy:

$$\frac{y\sqrt{k}}{\nu} > Re_v \;\Rightarrow\; \begin{cases} k_v &= k \\ y_v &= Re_v\nu/\sqrt{k_v} \end{cases} \tag{120}$$

$$\frac{y\sqrt{k}}{\nu} < Re_v \;\Rightarrow\; \begin{cases} k_v &= Re_v\sqrt{k}\nu/y \\ y_v &= y\sqrt{k_v}/\sqrt{k} \end{cases} \tag{121}$$

The constants, C (in the blending function), and Re_v are optimised using DNS-data [25]. The combination of $Re_v = 11$ and $C = 1.7$ gave the overall best results, as compared with DNS-data. The effect of these values is a rather narrow blending region, see Fig. 21. The calculated y_v^+ and k_v^+ using LRN $k-\omega$, [35] data (*a priori*) and the selected constants are shown in Fig. 22.

The new model is defined by Eqs. 116, 117, 118 119 and the blending function, f:

$$f = \exp^{-Re_t/1.7} \tag{122}$$

and the above routines for the specification of k_v and y_v.

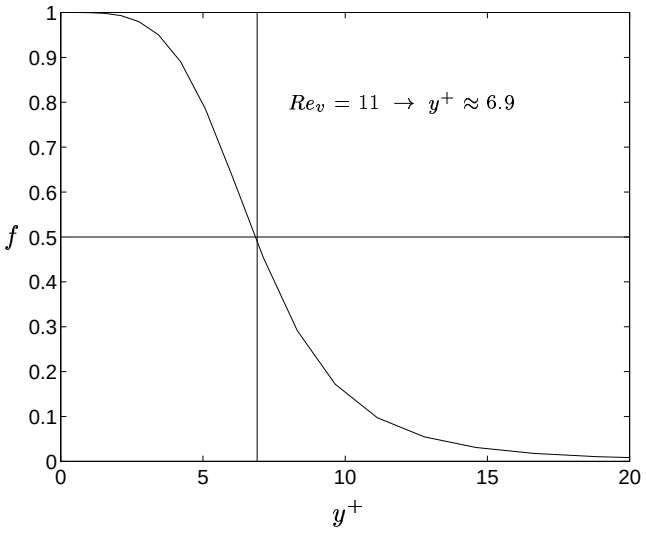

Figure 21: Blending function, f, using LRN $k-\omega$ data

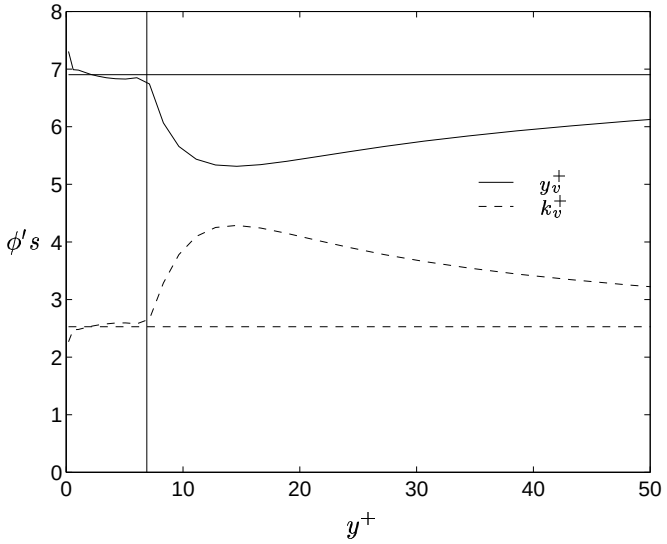

Figure 22: Comparison of the new models variation of viscous sub-layer quantities, with those given at $Re_v = 11 \rightarrow y^+ \approx 6.9$ (constant lines).

5 Modelling Near-wall Heat Transfer

In contrast to previous sections, this one is written in a brief and and abbreviated style. This is not to imply that the thermal field is any easier to predict or that the modelling is any simpler, but is merely a consequence of the lesser efforts made to improve the thermal models. To exemplify this, it can be noted that, in some predictions, an RSM turbulence model – which involves seven turbulent transport equations – is combined with a constant turbulent Prandtl number heat transfer model, i.e. a zero-equation isotropic model. The turbulent Prandtl number heat transfer model using the simple gradient diffusion hypothesis, or SGDH, relies on the similarity of the turbulence and heat transfer fields. The SGDH assumes that they are identical apart from a proportionality factor, the turbulent Prandtl number. The validity of this approximation in fully developed channel flow can be seen in Fig. 7. Using the SGDH approximation, it is also implied that the thermal field is isotropic. With an RSM the individual Reynolds stresses are known however, and can be used to predict the turbulent anisotropic level in the flow. If it is assumed that the anisotropicity of the heat transfer is identical to that of the turbulence, a GGDH, or Generalized Gradient Diffusion Hypothesis, model can be employed for the heat transfer prediction.

Although a GGDH would be more appropriate than a SGDH, the fundamental approximation of an identity between the flow field and thermal field is still used, and should be questioned. Similar to the turbulence field, it is also possible to solve a set of equations for thermal quantities. Examples of this approach are the two-equation model, $t^2 - \varepsilon_t$, of the Nagano group, Abe *et al.* [1] and EAHF (Explicit Algebraic Heat Flux) models of So and Sommer [30] and Dol *et al.* [11]. Here, however, only the simple model based on the turbulent Prandtl number is used.

5.1 Integration Method

The integrated or LRN method implies that the heat transfer is governed purely by viscous effects in the limit of the wall. The heat transfer is thus estimated using the Fourier law, such as:

$$q_l = -\lambda \frac{dT}{dy} = -\frac{C_p \mu}{Pr} \frac{dT}{dy} \tag{123}$$

where λ is the thermal conductivity given as $= C_p \mu / Pr$. The l in the heat flux indicates that it is the 'laminar' or the molecular part. Using the simple gradient diffusion hypothesis (SGDH) for the turbulent region, the 'turbulent' heat flux is computed as:

$$q_t = -\frac{C_p \mu_t}{Pr_t} \frac{dT}{dy} \tag{124}$$

The total heat transfer is then calculated by adding the two parts together, $q_{tot} = q_l + q_t$.

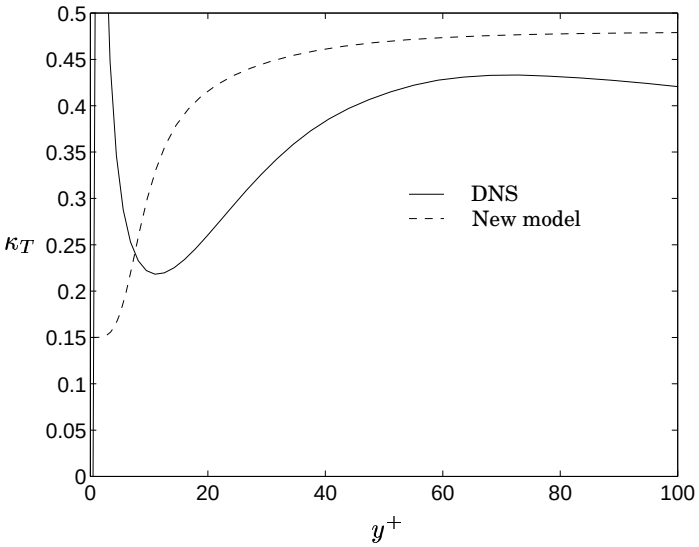

Figure 23: Coefficient, κ_T in log-law for temperature. Model Eq. 132 and DNS-data, $Re_\tau = 395$, [18].

Using a constant Prandtl number model, it is understood that all wall effects are embedded in the turbulence model, and hence any LRN modifications to the heat transfer model are normally excluded. However, as shown in Fig. 7, the turbulent Prandtl number is also affected by the wall, and there thus exists a number of heat transfer models that include some wall modifications, see e.g. Reynolds [28] and Kays [19].

5.2 Wall Function Method

The law-of-the-wall for the temperature was derived in section 3.2. From that the temperature profile in the inertial sub-layer is approximated with a logarithmic equation as given by Eq. 40:

$$T^+ \equiv \frac{T_w - T}{T_\tau} \equiv \frac{(T_w - T)\rho c u_\tau}{q_w} = \frac{1}{\kappa_T}\ln(y^+) + B_T \tag{125}$$

with $B_T = 3.9$ and $\kappa_T = 0.48$ for air ($Pr = 0.71$), see experimental data in Kader and Yaglom [16]. The reader is also referred to Huang and Bradshaw [12] and Kays and Crawford [20] for a recent discussions on the topic. Kawamura *et al.* [18] provide valuable DNS-data for the temperature equation in fully developed channel flow. The above relation for the wall temperature is not commonly used, however, and T^+ is instead expressed with the normalised velocity, $u^+ = U/u_\tau$, as:

$$T^+ = Pr_t(u^+ + Pr_f) \tag{126}$$

where $Pr_f = B_T/Pr_t - B$, and $Pr_t = \kappa/\kappa_T$, [16]. The constant, Pr_f, depends on the Prandtl number, which according to Jayatillaka [13] is:

$$\begin{aligned} Pr_f =& 9.24\left[\left(\frac{Pr}{Pr_t}\right)^{3/4} - 1\right] \\ & \left[1 + 0.28\exp\left(-0.007\frac{Pr_t}{Pr}\right)\right] \end{aligned} \tag{127}$$

5.3 New Blending Model

During the numerical optimisation of the new model it was found that the most appropriate blending parameter for the thermal field was the normalised temperature, T^+. The non-dimensionalised wall distance in Eq. 125, is however based on $y_p^* \equiv y_p\sqrt{k_p}\beta^{*1/4}/\nu$ instead of the commonly used although less satisfying y^+:

$$T^* = \frac{1}{\kappa_T}\ln(y^*) + B_T^* \tag{128}$$

T^* has not yet been given explicitly for the LRN region. Introducing normalised variables, $T^* = (T_w - T)\rho C_p\beta^{*1/4}\sqrt{k}/q_w$ and $y^* = y\beta^{*1/4}\sqrt{k}/\nu$, Eq. 123 can be re-written as:

$$q_w = \frac{C_p\rho\nu}{Pr}\frac{T^* q_w}{\rho C_p\beta^{*1/4}\sqrt{k}}\Big/\frac{y^*\nu}{\beta^{*1/4}\sqrt{k}} \tag{129}$$

Re-arranging, the linear law for temperature is given (see also Eq. 38):

$$T^* = Pr\,y^* \tag{130}$$

The non-dimensionalised temperature in the blending model thus becomes:

$$T^* = f Pr\, y_p^* + (1-f)\left[\frac{1}{\kappa_T} ln(y_p^*) + B_T\right] \tag{131}$$

where f is defined as for the turbulence field, see Eq. 108. To achieve accurate results with this heat transfer model in the case of a first node location in the buffer layer, the values of κ_T and B_T must be modified. This is not unreasonable since constant values are valid only in the logarithmic layer. In the new model, we chose to modify κ_T, which is reduced in the buffer layer, as found from DNS computations [18] and [17]. Reasonable agreement with the κ_T predicted by DNS was found for the relation:

$$\kappa_T = 0.33\left[1 - \exp(-Re_t/5)\right] + 0.15 \tag{132}$$

see Fig. 23. The expression gives $\kappa_T = 0.48$ in the logaritmic layer, as indicated by experimental data [12, 16, 20]. Note that the DNS-data ($Re_\tau = 395$) indicate a slightly lower value of $\kappa_T = 0.42$. There seems to be a Reynolds number dependency for this coefficient, however, as another DNS [17] ($Re_\tau = 150$) yields an even lower value, $\kappa_T = 0.36$.

Results obtained using this model are presented in Bredberg *et al.* [6].

Acknowledgments

Funding for the present work has been provided by STEM, the Volvo Aero Corporation and ALSTOM Power via the Swedish Gas Turbine Center.

References

[1] K. Abe, T. Kondoh, and Y. Nagano. A new turbulence model for predicting fluid flow and heat transfer in separating and reattaching flows - I. flow field calculations. *Int. J. Heat and Mass Transfer*, 37:139–151, 1994.

[2] R.S. Amano. Development of a turbulence near-wall model and its application to separated and reattached flows. *Numerical Heat Transfer*, 7:59–75, 1984.

[3] R.S. Amano, M.K. Jensen, and P. Goel. A numerical and experimental investigation of turbulent heat transport downstream from an abrupt pipe expansion. *J. Heat Transfer*, 105:862–869, 1983.

[4] J. Bredberg. Prediction of flow and heat transfer inside turbine blades using EARSM, $k-\varepsilon$ and $k-\omega$ turbulence models. Thesis for the Degree of Licentiate of Engineering, Dept. of Thermo and Fluid Dynamics, Chalmers University of Technology, Gothenburg, 1999. Also available at www.tfd.chalmers.se/~bredberg.

[5] J. Bredberg and L. Davidson. Prediction of flow and heat transfer in a stationary 2-D rib roughened passage using low-Re turbulent models. In *3:rd European Conference on Turbomachinery*, pages 963–972, London, 1999. IMechE.

[6] J. Bredberg, S-H. Peng, and L. Davidson. On the wall boundary condition for computing heat transfer with $k-\omega$ models. In J.H. Kim, editor, *HTD-Vol. 366-5, ASME Heat Transfer Divison - 2000*, volume 5, pages 243–250, Orlando, 2000. The American Society of Mechanical Engineers.

[7] C.C. Chieng and B.E. Launder. On the calculation of turbulent heat transfer transport downstream an abrupt pipe expansion. *Numerical Heat Transfer*, 3:189–207, 1980.

[8] M. Ciofalo and M. W. Collins. $k-\varepsilon$ predictions of heat transfer in turbulent recirculating flows using an improved wall treatment. *Numerical Heat Transfer, Part B*, 15:21–47, 1989.

[9] F.H. Clauser. The turbulent boundary layer. *Adv. Appl. Mech*, 4:1–51, 1954.

[10] L. Davidson and B. Farhanieh. CALC-BFC. Report 95/11, Dept. of Thermo and Fluid Dynamics, Chalmers University of Technology, Gothenburg, 1995.

[11] H.S. Dol, K. Hanjalić, and S. Kenjeres. A comparative assessment of the second-moment differential and algebraic models in turbulent natural convection. *Int. J. Heat Fluid Flow*, 18:4–14, 1997.

[12] P.G. Huang and P. Bradshaw. Law of the wall for turbulent flows in pressure gradients. *AIAA Journal*, 33:624–632, 1995.

[13] C.L.V. Jayatillaka. The influence of Prandtl number and surface roughness on the resistance of the laminar sublayer to momentum and heat transfer. *Progress in Heat and Mass Transfer*, 1:193, 1969.

[14] R.W. Johnson and B.E. Launder. Discussion of: On the calculation of turbulent heat transfer transport downstream an abrupt pipe expansion. *Numerical Heat Transfer*, 5:493–496, 1982.

[15] W.P. Jones and B.E. Launder. The prediction of laminarization with a two-equation model of turbulence. *Int. J. Heat and Mass Transfer*, 15:301–314, 1972.

[16] B.A. Kader and A.M. Yaglom. Heat and mass transfer laws for fully turbulent wall flows. *Int. J. Heat and Mass Transfer*, 15:2329–2351, 1972.

[17] N. Kasagi, Y. Tomita, and A. Kuroda. Direct numerical simulation of passive scalar in a turbulent channel flow. *J. Heat Transfer*, 114:598–606, 1992.

[18] H. Kawamura, H. Abe, and Y. Matsuo. DNS of turbulent heat transfer in channel flow with respect to Reynolds and Prandtl number effects. *Int. J. Heat and Fluid Flow*, 20:196–207, 1999.

[19] W.M. Kays. Turbulent Prandtl number - where are we? *J. Heat Transfer*, 116:284–295, 1994.

[20] W.M. Kays and M.E. Crawford. *Convective Heat and Mass Transfer*. McGraw-Hill, Inc, 1993.

[21] C.K.G. Lam and K.A. Bremhorst. Modified form of the $k-\varepsilon$-model for predicting wall turbulence. *J. Fluids Engineering*, 103:456–460, 1981.

[22] B.E. Launder. Numerical computation of convective heat transfer in complex turbulent flows: Time to abandon wall functions? *Int. J. Heat and Mass Transfer*, 27:1485–1491, 1984.

[23] B.E. Launder. On the computation of convective heat transfer in complex turbulent flows. *J. Heat Transfer*, 110:1112–1128, 1988.

[24] B.E. Launder and D.B. Spalding. The numerical computation of turbulent flows. *Computational Methods Appl. Mech. Eng.*, 3:269–289, 1974.

[25] R.D. Moser, J. Kim, and N.N. Mansour. Direct numerical simulation of turbulent channel flow up to Re=590. *Physics of Fluids*, 11:943–945, 1999. Data available at www.tam.uiuc.edu/Faculty/Moser/.

[26] V.C. Patel, W. Rodi, and G. Scheuerer. Turbulence models for near-wall and low Reynolds number flows: A review. *AIAA Journal*, 23:1308–1319, 1985.

[27] L. Prandtl. Zur turbulenten strömung in rohren und längs platten. Ergeb. Aerod. Versuch, Göttingen, IV Lieferung, 18, 1932.

[28] A.J. Reynolds. The prediction of turbulent Prandtl and Schmidt numbers. *Int. J. Heat and Mass Transfer*, 18:1055–1069, 1975.

[29] A. Sahay and K.R. Sreenivasan. The wall-normal position in pipe and channel flows at which viscous and turbulent shear stresses are equal. *Physics of Fluids*, 11:3186–3188, 1999.

[30] R.M.C So and T.P. Sommer. An explicit algebraic heat-flux model for the temperature field. *Int. J. Heat and Mass Transfer*, 39:455–465, 1996.

[31] H. Tennekes and J.L. Lumley. *A First Course in Turbulence*. Massachusetts Institute of Technology, Cambridge, 1972.

[32] A.A. Townsend. *The structure of turbulent shear flow*. Cambridge University Press, Cambridge, 1976.

[33] T. von Karman. Mechanishe ähnlichkeit un turbulenz. Nachr. Ges. Wiss., Göttingen, pp 68, 1930.

[34] D.C. Wilcox. Reassessment of the scale-determining equation for advanced turbulence models. *AIAA Journal*, 26:1299–1310, 1988.

[35] D.C. Wilcox. Comparison of two-equation turbulence models for boundary layers with pressure gradient. *AIAA Journal*, 31:1414–1421, 1993.

[36] D.C. Wilcox. *Turbulence Modeling for CFD*. DCW Industries, Inc., 1993.